GENESIS OF DIOCTAHEDRAL K- AND Na-BEARING MICAS AT THE STRONGLY ALTERED LATE PROTEROZOIC UNCONFORMITY OF THE TANDILIA BELT, CENTRAL-EASTERN ARGENTINA

Juan C. MARTÍNEZ[1], Hans J. MASSONNE[2], Jorge A. DRISTAS[3] y María C. FRISICALE[1]

[1] CONICET-INGEOSUR and Departamento de Geología, San Juan 670, UNS, Bahía Blanca, 8000, Argentina*.
[2] Institut für Mineralogie und Kristallchemie, Universität Stuttgart, Azenbergstrasse 18, D-70174, Germany.
[3] CIC, INGEOSUR and Departamento de Geología, San Juan 670, UNS, Bahía Blanca, 8000, Argentina.
* Corresponding author Dr. Juan Cruz Martínez: jcmartin@uns.edu.ar

ABSTRACT

The unconformity-related phyllosilicate mineral assemblages of the most pervasively altered basement of the Tandilia belt, central Buenos Aires Province, were studied from two ~50 km distant areas, Barker and San Manuel. The secondary dioctahedral K-white micas show a compositional spread probably by a solid-solution towards pyrophyllite. In addition, electron microprobe analyses of micas yielded widely variable Na* [Na/(Na+K+Ca+Ba)] ratios, which can be related to a compositional range between nearly pure muscovite and intermediate micas with maximum paragonite contents corresponding to muscovite$_{55}$paragonite$_{45}$ and muscovite$_{40}$ paragonite$_{60}$ for the Barker and San Manuel areas, respectively. Scanning electron images suggest the local occurrence of paragonite/intermediate K-Na white micas, finely intergrown within secondary K-white mica and pyrophyllite. P-T pseudosections (H_2O saturated) in the Na-K-Fe-Mg-Mn-Al-Si-Ti-O-H system for different XFe^{3+} (Fe^{+3}/Fe_{tot}) constrain temperatures of formation of the secondary mineral assemblages around 280 - 340 ºC, whereas such mineral assemblages are almost insensitive to pressure between 0.5 and 5 kbar. At these P-T conditions, the most likely mineral assemblages include K-white mica, chloritoid, rutile, and hematite (± pyrophyllite ± paragonite). An additional phase is either quartz, which was observed as relic of the protolith, or diaspore. A $^{40}Ar/^{39}Ar$ step-heating age of 630 ± 30 Ma on a K-white mica rich sample linked the hydrothermal alteration event to the Brasiliano orogenic cycle.

Keywords: *K-Na bearing micas, altered basement, Tandilia Late Proterozoic Unconformity, $^{40}Ar/^{39}Ar$ step-heating thermochronology, thermodynamic modeling*

RESUMEN

Génesis de micas dioctahédricas con Na y K del basamento intensamente alterado de la discordancia del Proterozoico Tardío de Tandilia, centro-este de Argentina

Las asociaciones de minerales filosilicáticos de la discordancia del basamento más intensamente alterado de Tandilia, centro de la provincia de Buenos Aires, fueron estudiadas y comparadas en dos áreas distantes por ~50 km, Barker y San Manuel. Las micas dioctahédricas potásicas de la alteración tienen una variación composicional debida probablemente a solución sólida hacia pirofilita. Además, los análisis de dichas micas tienen valores de Na* [Na/(Na+K+Ca+Ba)] ampliamente variables, los cuales se pueden vincular a un rango de composiciones entre muscovita pura y micas intermedias, con un máximo contenido de paragonita correspondiente a: muscovita$_{55}$paragonita$_{45}$ y muscovita$_{40}$ paragonita$_{60}$, respectivamente para las áreas de Barker y San Manuel. Las imágenes de escaneado electrónico sugieren la ocurrencia local de paragonita/micas intermedias con K-Na finamente intercrecidas dentro de las micas potásicas y pirofilitas secundarias. Las pseudosecciones de presión - temperatura (con H_2O saturada) generadas para el sistema Na-K-Fe-Mg-Mn-Al-Si-Ti-O-H, con diferentes XFe^{3+} (Fe^{+3}/Fetot), permiten definir temperaturas mínimas de formación para las paragénesis de minerales de alteración entre 280 - 340 ºC, mientras que dichas paragénesis son prácticamente insensibles a los cambios de presión entre 0,5 y 5 kbar. En estas condiciones, las paragénesis de minerales de alteración más probables que surgen del modelado incluyen mica potásica, cloritoide, rutilo y hematita (± pirofilita ± paragonita). Como fases adicionales se hallan cuarzo, relíctico del protolito, o diasporo. Una edad de 630 ± 30 Ma, determinada por calentamiento escalonado Ar^{40}/Ar^{39} en una muestra rica en mica potásica secundaria, vincula el evento de alteración hidrotermal al ciclo orogénico Brasiliano.

Palabras clave: *Micas con K y Na, basamento alterado, discordancia del Proterozoico Tardío de Tandilia, termocronología Ar^{40}/Ar^{39}, modelado termodinámico*

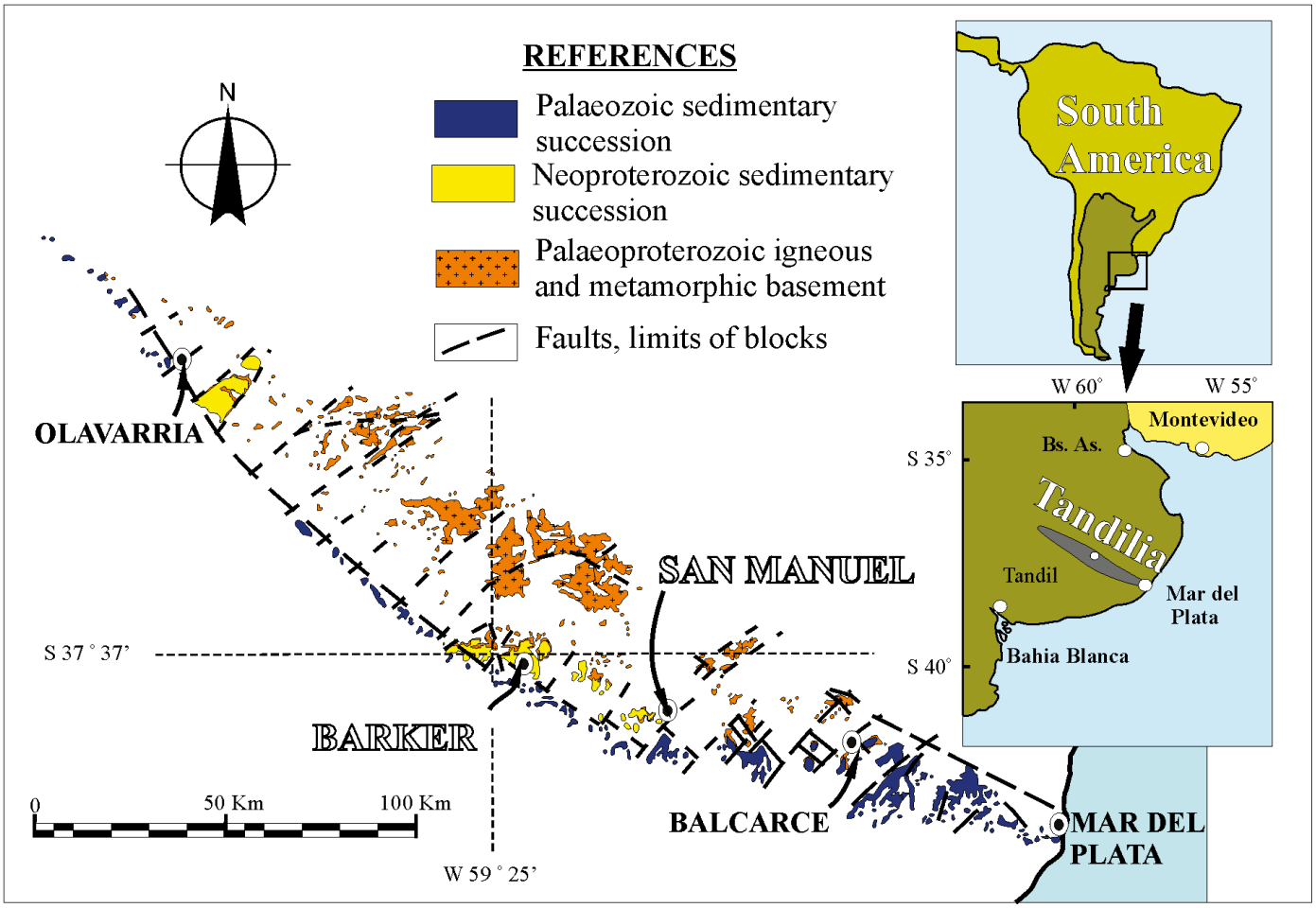

Figure 1: Overview geologic map of the Tandilia belt with localities of interest (modified from Iñiguez-Rodríguez *et al.* 1989, Poiré and Spalletti 2005).

INTRODUCTION

K-Na-bearing micas such as paragonite, brammallite (Na-illite), metastable intermediate K-Na white micas, intergrowth or mixed-layered K-white mica and paragonite are known to occur in very low grade metamorphic sequences (e.g., Frey 1969; Kisch 1983; Frey 1987; Li *et al.*. 1994; Livi *et al.* 1997; Merriman and Peacor 1999; Merriman and Frey 1999; Merriman 2002; Árkai *et al.* 2003; Árkai *et al.* 2008). In addition, the formation of such dioctahedral phyllosilicates has also been reported from alteration of precursor minerals in hydrothermal environments (e.g., Shau *et al.* 1991; Jiang and Peacor 1993; Monecke *et al.* 2001; Giorgetti *et al.* 2003).

Conditions of pressure (P) and temperature (T) of the formation of the above dioctahedral micas were hitherto rarely deduced by thermodynamic modeling. For instance, this method was applied to naturally occurring mineral assemblages with paragonite from Alpine and Variscan low-T metamorphic terrains (Árkai *et al.* 2008). In previous studies of K-Na-bearing micas, such as those mentioned above, the recognition of textures and the way such fine-grained layer-silicates appear in mineral assemblages were systematically tackled by means of electron microscopic techniques: transmission electron microscopy (TEM), scanning electron microscopy (SEM), electron microprobe (EMP) analyses, analytical electron microscopy (AEM); and by the most traditionally used technique of X-ray powder diffractometry (XRD).

In the Tandilia belt (Fig. 1) phyllosilicate assemblages of alterations are restricted to the unconformity zone between an igneous-metamorphic Palaeoproterozoic basement and an overlying mainly siliciclastic Neoproterozoic sedimentary succession. These assemblages have been studied for more than three decades in the Barker and San Manuel areas (Dristas and Frisicale 1984; Regalía 1987; Zalba *et al.* 1992; Frisicale and Dristas 1993; Zalba and Andreis 1998; Dristas *et al.* 2003; Dristas and Martínez 2007; Martínez and Dristas 2007; Martínez *et al.* 2010; Fernández *et al.* 2010). However, the finding of locally occurring dioctahedral K-Na-bearing micas was only possible by a systematic XRD study of samples from several alteration profiles combined with EMP analyses and analyses of bulk-rock mass changes (Martínez *et al.* 2010).

This work is aimed at explaining the genesis of the local occurrence of dioctahedral K-Na-bearing micas in secondary mineral assemblages, which developed

over the basement in a restricted zone (1 - 15 m: below the unconformity) in two distant areas (~50 km between Barker and San Manuel). For doing this, three main topics were considered. The first one was related to the characterization of the chemistry and arrangement of these micas. The usage of XRD technique was limited by the very low amount of paragonite and/or any other Na-bearing mica in the studied samples. Thus, EMP analyses and backscattered SEM imagery were carried out in order to chemically characterize K-white micas and adjacent pyrophyllite and to texturally recognize different mineral phases. The second topic referred to the physical conditions, pressure and temperature, of formation of the mineral assemblages with these phyllosilicates. Thermodynamic modeling of a selected bulk-rock predicts stability fields for mineral assemblages containing pyrophyllite, K-white mica, paragonite, quartz, rutile, hematite, kaolinite and diaspore, thus, allowing P-T estimates. The advantage of this research is the possibility to apply it also to the most leached and in situ altered migmatitic-gneissic rocks of the basement at the unconformity, where corroded quartz and zircon are the only remnants of pre-existing metamorphic minerals. Therefore, there was no need to perform models on specific bulk-rocks as in Árkai *et al.* (2008). Unraveling the thermo-tectonic event linked to the formation of this type of K-bearing alteration was the third topic, which has been accomplished by $^{40}Ar/^{39}Ar$ step-heating thermochronology on a K-rich altered sample.

GEOLOGICAL SETTING AND PETROGRAPHY OF STUDIED SAMPLES

The Tandilia belt is the southernmost exposition of the Río de la Plata craton located in the central Buenos Aires province, central-eastern Argentina. This belt, being 350 km long and up to 60 km wide, is composed of two major units, an igneous-metamorphic basement and an overlying sedimentary succession (Fig. 1). The basement rocks are known as Buenos Aires Complex (BAC, Marchese and Di Paola 1975). The BAC is largely composed of granitoids, granitic to tonalitic gneisses and migmatites. Subordinated rocks of this igneous-metamorphic complex are amphibolites, ultramafic rocks, calc-silicate rocks and scarce schists. The formation and main tectonic evolution of the BAC is attributed to a continent-continent collision during the Trans-Amazonian orogenic cycle, spanning mainly 2.2-1.8 Ga (Cingolani and Dalla Salda 2000; Cingolani *et al.* 2002; Hartmann *et al.* 2002; Pankhurst *et al.* 2003; Cingolani *et al.* 2005; Massonne *et al.* 2012). Two suites of calc-alkaline (andesitic to rhyolitic) and tholeiitic (basaltic) dykes intruded the BAC during the Early Proterozoic (2.0 Ga.) and Middle Proterozoic (1.6 Ga), respectively (Iacumin *et al.* 2001; Teixeira *et al.* 2002; Dristas *et al.* 2013). The western and southwestern outcrops of the BAC are unconformably overlaid by subhorizontal Neoproterozoic to Early Palaeozoic shallow marine siliciclastic and carbonatic sedimentary rocks (Dalla Salda and Iñiguez-Rodríguez 1979; Iñiguez-Rodríguez *et al.* 1989; see Fig. 1). This sedimentary succession reached diagenetic temperatures not higher than 200°C at its lower section (Gómez Peral *et al.* 2011). The age of sedimentation/diagenesis of the lower sedimentary unit (Villa Mónica Formation), overlying the igneous-metamorphic basement, was estimated to be (1) between 800-900 Ma (Poiré 1987) by biostratigraphy with stromatolite fossils, (2) 793 ± 32 Ma by a Rb/Sr isochron (Cingolani and Bonhomme 1988) and (3) 787 ± 22 Ma by the K/Ar dating method on bulk-rocks (Dristas and Martínez 2007). The structure of the Tandilia belt is characterized by fault-limited blocks with evidences of Neoproterozoic vertical movements (Iñiguez-Rodríguez *et al.* 1989; Sellés-Martínez 1993).

In the Barker area, nine profiles of alteration were studied at the Tandilia late Proterozoic unconformity (TLPU) zone between the BAC and the overlying sedimentary rocks (Martínez and Dristas 2007; Martínez *et al.* 2010). In the east of the range of Cuchilla de las Aguilas (Fig. 2a), the basement is composed of banded migmatites with interbedded amphibolite lenses which are less than 1.5 m wide and up to 20 m long. These rocks show a regional subvertical foliation striking west-north-west (N70ºW to N60ºW). The leucosomes of these migmatites are dominated by plagioclase (andesine) and orthoclase with scarce microcline, whereas the melanosomes are mainly composed of biotite. Accessory minerals include garnet, apatite, zircon, allanite, monazite and Ti-Fe oxide minerals. At the unconformity, in the east of Cuchilla de Las Aguilas - La Tolva (Fig. 2a), the intensely altered migmatite consists of granoblastic quartz relicts, with marked dissolution embayments, floating in a groundmass of K-white micas (2M1-1M), rutile, tourmaline, aluminium phosphate sulphate (APS) minerals and goethite-hematite (Martínez and Dristas 2007; Martínez *et al.* 2010).

Another profile of alteration in the Barker area, characterized by Na enrichment in the phyllic alteration (Martínez and Dristas 2007), is the one at the Inca Huasi ranch (Fig. 2a). According to Martínez and Dristas (2007), the basement of this sector is characterized by a granitic to tonalitic banded migmatite with xenoblastic texture. Biotite is pseudomorphically replaced by muscovite; andesitic plagioclase shows colonies of myrmekite and is subordinated to K-feldspar. A profile of ~6 metres of alteration is discernable in a small quarry at the TLPU of this sector. The alteration of this profile is characterized by an alteration pattern transitional between the mineral association: (1) K-white mica + chlorite + calcite + rutile + hematite/goethite farther from the unconformity and (2) K-white mica + pyrophyllite + paragonite/intermediate K-Na mica + rutile + hematite/goethite + APS minerals + tourmaline ± kaolinite closer to the unconformity (Martínez *et al.* 2010). This pattern of alteration is commonly repeated in the other profiles of alteration, which affected also the base of the sedimentary sequence (e.g., Dristas and Martínez 2007; Martínez and Dristas 2007).

More than 50 kilometres southeastwards

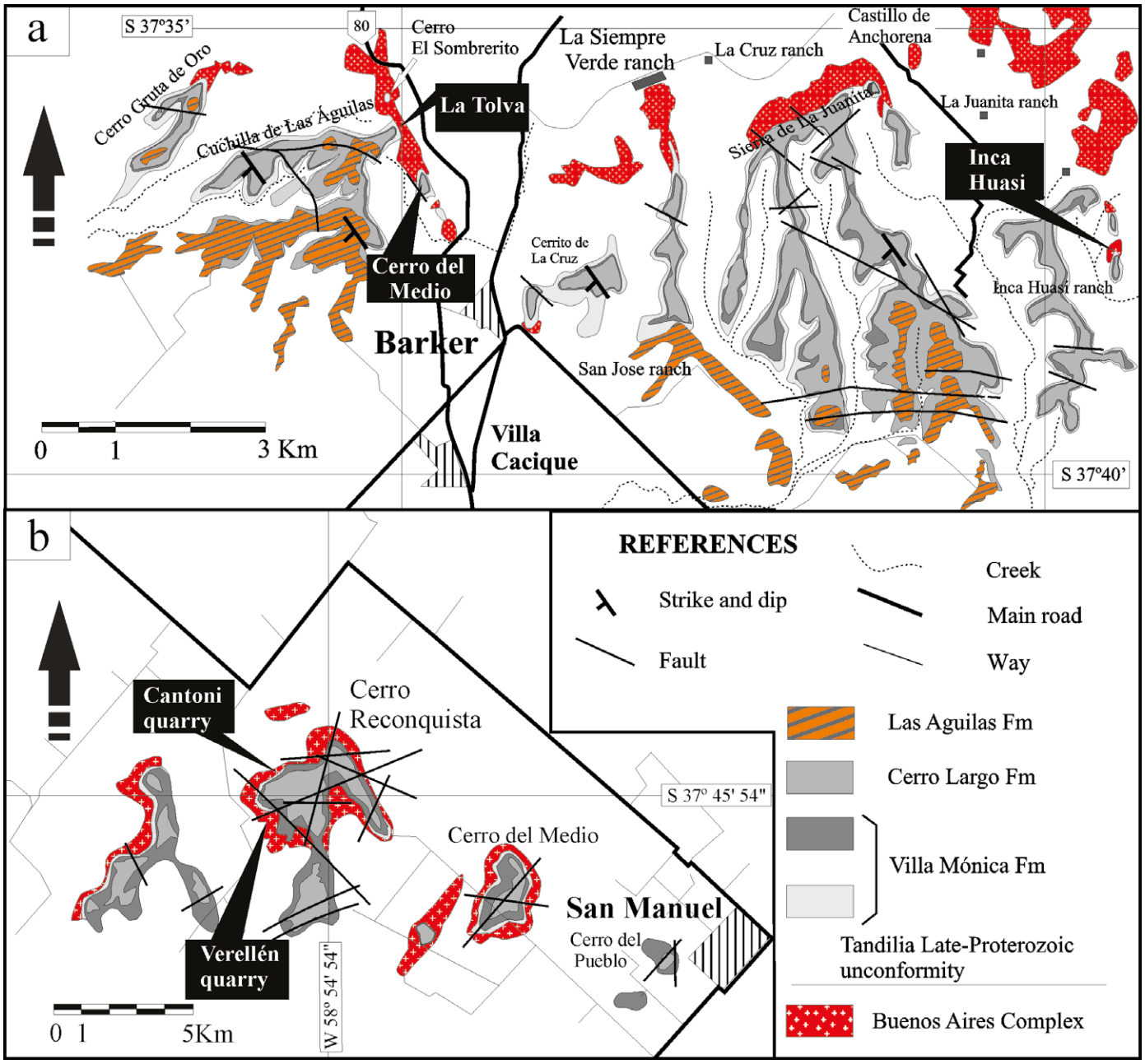

Figure 2: Geologic map of the Barker; a) and San Manuel; b) areas with sampling locations cited in the text.

from the Barker area (Fig.1) the alteration at the TLPU, subject of this study, is well exposed in many quarries at the hills (Fig.2b) located to the west of San Manuel. The altered basement of this area was early studied by Dristas and Frisicale (1984), Regalía (1987) and Zalba *et al.* (1992) and more recently by Fernández *et al.* (2010). According to these authors more than 15 m of altered basement, without exposition of the unaltered protolith in the neighboring area, can be registered below the unconformity. Migmatitic banding and ptigmatic folds are remnants in the altered basement rocks (Dristas and Frisicale 1984). The main mineral association of the altered basement near the unconformity essentially consists of pyrophyllite + K-white mica + goethite/hematite ± kaolinite. Quartz is relictic and completely corroded when diaspore is present. Accessory secondary minerals are tourmaline, rutile, and APS minerals. Further away from the unconformity kaolinite is rather absent and K-white mica dominates over pyrophyllite (Dristas and Frisicale 1984; Fernandez *et al.* 2010).

ANALYTICAL METHODS

Alteration textures of the most altered rocks at the unconformity were studied by optical microscopy in more than 30 samples. Samples were surveyed in many field trips to several alteration profiles from the San Manuel (Canttoni quarry

and Verellén quarry in Cerro Reconquista) and Barker (La Tolva-Cerro del Medio and Inca Huasi) areas (Fig. 2a-b). These profiles of alteration and their mineralogical variations were already published by Martínez and Dristas (2007) and Fernández *et al.* (2010), for the Barker and San Manuel areas, respectively. In this work we deal with chemical analyses of K-white mica and pyrophyllite of the most intensely altered basement at the TLPU published in Martínez *et al.* (2010) for the two representative localities of the Barker area and new data for phyllosilicates at the TLPU of the San Manuel area. For doing this, selected polished thin-sections of phyllosilicate-rich samples from the San Manuel area were investigated at the Institut für Mineralogie und Kristallchemie, Universität Stuttgart (Germany) by acquiring quantitative and qualitative analyses with a Cameca SX100 EMP equipped with five wavelength-dispersive spectrometers (take off angle of 40º). In order to avoid elemental diffusion, Na and K were analysed first. The following natural standards were used: wollastonite (Ca, Si), hematite (Fe), albite (Na), orthoclase (K) rhodonite (Mn) and barite (Ba). Synthetic standards were: periclase (Mg), corundum (Al) and rutile (Ti). A voltage of 15 kV was often combined with a beam current of 10 nA and a beam diameter of 2-3 μm. The chemical formulae of K-white mica and pyrophyllite of the most altered basement at the TLPU were calculated based on 22 positive charges ignoring H_2O which cannot be determined by the electron microprobe. All iron obtained by EMP in K-white micas and pyrophyllite was recast as Fe^{3+} since these micas coexist with hematite. Besides, for K-white micas this assumption is supported by a total number of octahedral cations ≥ 2 when all iron is considered as Fe^{3+} (see Livi *et al.* 1997). Only analyses with calculated oxide contents > 93%, Si > 3.00 a.p.f.u. (atoms per formula unit), and Ca < 0.05 a.p.f.u. were considered.

Selected thin-sections were gold-coated and their texture were studied using a LEO (Zeiss) 1530 Gemini high-resolution thermally aided Field Emission SEM at Institut für Geologie, Mineralogie and Geophysik, Ruhr-Universität Bochum, Germany. The SEM was operated with an acceleration voltage of 20 kV for image capturing.

Among the samples analysed with the EMP, three samples of the most altered rocks at the unconformity were selected for bulk-rock analyses which were performed by ACTLABS (Activation laboratories Ltd., Ontario, Canada). Samples were mixed with lithium metaborate and lithium tetraborate and fused in an induction furnace. The obtained melt was immediately poured into a solution of 5% nitric acid containing an internal standard, and mixed continuously until complete dissolution (~30 minutes). The samples were analysed for major oxides on a Varian Vista 735 ICP. The sample solution was spiked with internal standards to cover the entire mass range. They were further diluted and introduced into a Perkin Elmer SCIEX ELAN 9000 ICP-MS using a proprietary sample introduction methodology.

One sample rich in K-white mica was selected for $^{40}Ar/^{39}Ar$ dating by step-heating. The whole-rock chip for $^{40}Ar/^{39}Ar$ analysis was processed at the Arizona Nobel Gases Laboratory (ANGL) and irradiated at the USGS TRIGA Reactor, Denver, Colorado along with the flux monitors to calculate J-factors and K_2SO_4 and CaF_2 salts to calculate correction factors for interfering neutron reactions. Following a 2 to 3 week cooling period to allow for the decay of short-lived isotopes, the sample was loaded into the arms of a glass storage tree above a double-vacuum, resistance-heated furnace and heated to 120°. At the same time the entire extraction line was hold for 48 hours at 220°C. Getters and furnace were independently degassed near the end of the process. The sample was then dropped into the furnace and argon was extracted using a computer controlled step-heating routine. The temperature of the furnace is estimated to be accurate to ± 20°C. The duration time of each step-heating was 12 minutes followed by a cool down to 500°C prior to advancing the gas into two successive gettering stages for argon purification. The argon was then admitted into a VG 5400 mass spectrometer, where it was ionized and detected by a VG electron multiplier and digitized with a Keithley 617 Electrometer. Data collection and processing were accomplished using the computer program Mass Spec (Deino 2001). The decay constants used were those recommended by Renne *et al.* (2010). Baseline values were subtracted and the isotopic measurements then were regressed to time zero using standard linear regression techniques. Additional corrections and associated uncertainties were applied to account for blanks, machine discrimination, atmospheric contribution, and interfering isotopes produced in the reactor from Ca, K and Cl present in the samples.

RESULTS

Chemistry of K-white mica and pyrophyllite

Chemical compositions representative of K-white mica and pyrophyllite, determined with the EMP, from the three compared localities are given in tables 1a-b. Two of these localities are situated in the Barker area: east of Cuchilla de las Aguilas (includes La Tolva and Cerro del Medio) and Inca Huasi (Fig. 2a). The third one is in the San Manuel area: Cerro Reconquista (Cantoni and Verellén quarries, figure 2b). Based on the classification schema proposed in an IMA subcommittee report (Rieder *et al.* 1998), the studied secondary K-white micas are true micas, since more than 50% of the total interlayer cations (t.i.c. = K+Na+Ca+Ba p.f.u.) are monovalent, and dioctahedral subgroup micas containing less than 2.5 octahedral cations (Martínez *et al.* 2010). According to the classification parameters (Si: 3.0-3.1; $R^{2+}/(R^{2+} + R^{3+}) < 0.25$; ^{VI}Al: 1.9-2.0; $^{VI}Al/(^{VI}Al+Fe^{3+})$: 0.5-1.0) proposed in Rieder *et al.* (1998), these micas mainly show compositions close to that of ideal muscovite (Figs. 3a). The Si (a.p.f.u) contents of K-white micas from the San Manuel area range from 3.04 to 3.18 showing a wider range than in rep-

TABLE 1a: Representative chemical compositions and calculated formulae of K-white micas (Kwm) determined by EMP. Abbreviations: San Manuel (SM) and Inca Huasi (IH), total interlayer charge = t.i.c (Na+K+Ca+Ba), Na/(Na+K+Ca+Ba) (Na*), number of analysis (#).

Area/Sample nº	SM / 0110 Kwm				SM / 0410 Kwm			SM / 1110 Kwm			IH / 1324 Kwm				
Elements (wt%)	#29	#30	#37	#38	#58	#61	#63	#11	#27	#28	#4	#6	#19	#35	#37
SiO_2	47.12	47.57	46.99	46.90	46.20	46.47	46.32	46.46	46.87	46.30	48.10	49.29	47.78	48.13	47.10
TiO_2	0.00	0.00	0.00	0.01	0.00	0.00	0.01	0.02	0.06	0.07	0.01	0.01	0.02	0.02	0.02
Al_2O_3	37.67	37.58	35.96	36.80	37.24	37.63	37.11	37.01	36.28	36.76	37.62	37.86	37.80	37.60	38.07
Fe_2O_3	0.40	0.49	0.50	0.21	0.91	0.61	0.95	0.22	0.89	0.73	0.86	0.55	0.70	0.78	0.68
MgO	0.02	0.00	0.24	0.06	0.04	0.04	0.02	0.18	0.01	0.00	0.06	0.04	0.04	0.05	0.01
MnO	0.00	0.03	0.00	0.00	0.00	0.00	0.00	0.00	0.00	0.00	0.01	0.00	0.00	0.00	0.00
CaO	0.04	0.04	0.18	0.41	0.01	0.05	0.01	0.00	0.00	0.01	0.03	0.06	0.01	0.04	0.02
BaO	0.11	0.11	0.00	0.03	0.08	0.01	0.01	0.01	0.19	0.19	0.09	0.06	0.29	0.06	0.08
Na_2O	3.41	2.22	0.53	0.10	2.31	3.41	1.08	0.19	0.86	0.81	0.62	2.91	2.04	1.82	1.76
K_2O	5.40	6.70	9.37	10.20	7.53	5.90	9.34	10.59	9.18	9.50	8.96	5.52	7.20	7.23	7.78
Total	94.17	94.74	93.77	94.72	94.32	94.12	94.85	94.68	94.34	94.37	96.36	97.44	95.88	95.73	95.52
Cations															
Si	3.082	3.102	3.130	3.103	3.054	3.055	3.062	3.072	3.104	3.075	3.109	3.141	3.092	3.111	3.065
$Al^{(IV)}$	0.918	0.898	0.870	0.897	0.946	0.945	0.938	0.928	0.896	0.925	0.891	0.859	0.908	0.889	0.935
$Al^{(VI)}$	1.987	1.991	1.952	1.973	1.955	1.970	1.954	1.956	1.936	1.953	1.975	1.984	1.976	1.976	1.985
Ti	0.000	0.000	0.000	0.000	0.000	0.000	0.001	0.001	0.003	0.003	0.000	0.000	0.001	0.001	0.001
Fe^{3+}	0.020	0.024	0.025	0.010	0.045	0.030	0.047	0.011	0.044	0.037	0.042	0.026	0.034	0.038	0.033
Mn	0.000	0.001	0.000	0.000	0.000	0.000	0.000	0.000	0.000	0.000	0.000	0.000	0.000	0.000	0.000
Mg	0.002	0.000	0.024	0.006	0.004	0.004	0.002	0.018	0.000	0.000	0.006	0.003	0.004	0.005	0.001
Sum VI	1.989	1.992	1.976	1.980	1.959	1.974	1.956	1.975	1.942	1.959	1.982	1.988	1.981	1.982	1.987
Ca	0.002	0.003	0.013	0.029	0.001	0.004	0.000	0.000	0.000	0.001	0.002	0.004	0.001	0.003	0.001
Na	0.432	0.281	0.068	0.013	0.213	0.434	0.138	0.025	0.110	0.104	0.078	0.360	0.255	0.228	0.222
K	0.451	0.557	0.796	0.861	0.739	0.494	0.788	0.893	0.775	0.805	0.739	0.449	0.594	0.596	0.646
Ba	0.011	0.011	0.000	0.003	0.010	0.001	0.001	0.001	0.020	0.020	0.009	0.006	0.029	0.006	0.008
t.i.c	0.896	0.852	0.878	0.905	0.940	0.933	0.928	0.986	0.944	0.944	0.828	0.819	0.880	0.834	0.877
Na*	0.482	0.330	0.078	0.014	0.315	0.465	0.149	0.027	0.122	0.112	0.094	0.439	0.290	0.274	0.253
Si/Al(tot)	1.061	1.074	1.109	1.081	1.053	1.915	1.059	1.065	1.096	1.069	1.866	1.105	1.072	1.086	1.050

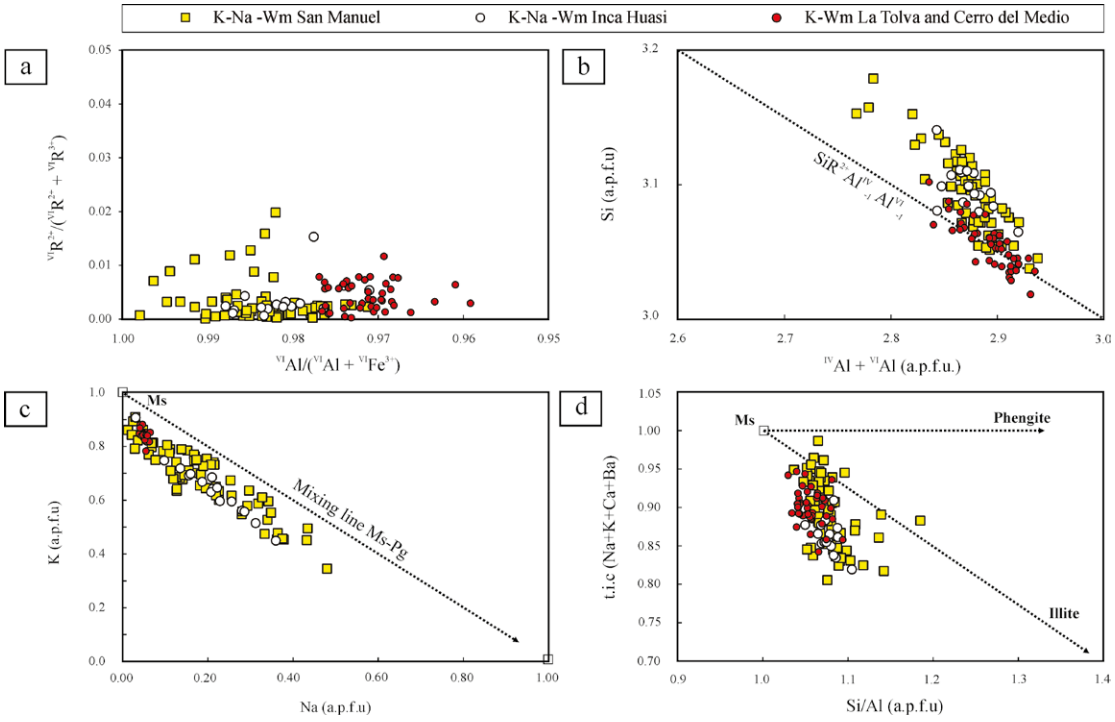

Figure 3: Compositional variation of cations and ratios of dioctahedral K-white micas of the studied rocks based on EMP data. Empty squares for muscovite (Ms) end member.

TABLE 1b: Representative chemical compositions and calculated formulae of K-white micas (Kwm) and pyrophyllites (Prl) determined by EMP. Abbreviations: La Tolva (LT), Cerro del Medio (CM), Inca Huasi (IH), San Manuel (SM), total interlayer charge = Na+K+Ca+Ba (t.i.c), Na/(Na+K+Ca+Ba) (Na*), number of analysis (#).

Area/Sample nº	LT / 0904 Kwm			CM / 0322 Kwm		SM / 0110 Prl		SM / 0410 Prl		SM / 1110 Prl		IH / 1324 Prl			
Elements (wt%)	#2	#5	#12	#7	#10	#8	#23	#5	#11	#31	#37	#8	#14	#15	#24
SiO_2	46.61	45.88	46.40	46.76	46.96	64.00	64.66	61.77	64.77	61.04	65.53	62.18	60.21	57.36	66.92
TiO_2	0.05	0.05	0.13	0.03	0.04	0.03	0.00	0.00	0.00	0.01	0.01	0.02	0.02	0.02	0.00
Al_2O_3	37.11	36.83	36.69	36.91	37.04	30.59	29.79	30.83	28.46	30.76	28.68	31.57	33.02	34.99	29.30
Fe_2O_3	0.96	1.64	1.47	1.08	0.93	0.03	0.03	0.03	0.02	0.03	0.04	0.05	0.03	0.04	0.02
MgO	0.12	0.06	0.05	0.12	0.16	0.00	0.01	0.03	0.00	0.03	0.02	0.05	0.03	0.08	0.00
MnO	0.00	0.00	0.02	0.01	0.00	0.00	0.00	0.01	0.03	0.00	0.01	0.00	0.00	0.00	0.06
CaO	0.07	0.01	0.01	0.08	0.13	0.12	0.02	0.25	0.02	0.09	0.05	0.07	0.06	0.07	0.02
BaO	0.00	0.05	0.08	0.01	0.02	0.00	0.00	0.01	0.00	0.01	0.00	0.00	0.04	0.02	0.01
Na_2O	0.43	0.32	0.33	1.34	1.44	0.50	0.21	0.42	0.21	0.98	0.25	0.48	1.22	1.97	0.19
K_2O	9.28	10.39	10.15	8.45	7.89	0.51	0.34	0.33	0.09	1.56	0.44	2.44	2.19	1.35	0.21
Total	94.63	95.23	95.33	94.79	94.61	95.77	95.06	93.68	93.60	94.51	95.03	96.86	96.80	95.90	96.73
Cations															
Si	3.078	3.043	3.066	3.080	3.086	3.845	3.898	3.795	3.954	3.758	3.951	3.749	3.648	3.512	3.956
$Al^{(IV)}$	0.922	0.957	0.934	0.920	0.914	0.155	0.102	0.205	0.046	0.242	0.049	0.251	0.352	0.488	0.044
$Al^{(VI)}$	1.967	1.922	1.924	1.945	1.957	2.011	2.015	2.029	2.002	1.990	1.989	1.993	2.006	2.038	1.998
Ti	0.002	0.002	0.006	0.001	0.002	0.001	0.000	0.000	0.000	0.001	0.000	0.001	0.001	0.001	0.000
Fe^{3+}	0.048	0.082	0.073	0.054	0.046	0.001	0.001	0.001	0.001	0.001	0.002	0.002	0.001	0.002	0.001
Mn	0.000	0.000	0.001	0.000	0.000	0.000	0.000	0.000	0.001	0.000	0.001	0.000	0.000	0.000	0.003
Mg	0.011	0.006	0.005	0.012	0.016	0.000	0.001	0.002	0.000	0.002	0.001	0.004	0.002	0.007	0.000
Sum VI	1.980	1.930	1.937	1.959	1.975	2.013	2.015	2.032	2.003	1.994	1.992	1.998	2.009	2.046	2.001
Ca	0.005	0.001	0.001	0.006	0.009	0.008	0.001	0.016	0.001	0.006	0.003	0.005	0.004	0.005	0.001
Na	0.055	0.041	0.042	0.171	0.184	0.058	0.025	0.050	0.025	0.117	0.029	0.056	0.143	0.234	0.022
K	0.782	0.879	0.856	0.710	0.662	0.039	0.026	0.025	0.007	0.122	0.034	0.188	0.169	0.106	0.016
Ba	0.000	0.005	0.008	0.001	0.002	0.000	0.000	0.001	0.000	0.001	0.000	0.000	0.004	0.002	0.001
t.i.c	0.841	0.925	0.907	0.888	0.857	0.105	0.052	0.092	0.033	0.251	0.067	0.249	0.320	0.347	0.040
Na*	0.065	0.044	0.047	0.193	0.215										
Si/Al(tot)	1.066	1.057	1.073	1.075	1.075										
Si/R^3						1.774	1.840	1.698	1.930	1.683	1.937	1.670	1.546	1.390	1.937

resentative samples from the Barker area (Fig. 3b, Inca Huasi, La Tolva and Cerro del Medio). Besides, total Al (a.p.f.u) of the former micas is also slightly more scattered to lower values (> 2.7) than in K-white micas from the Barker area (> 2.84) (Fig. 3b). K-white micas from east of Cuchilla de las Aguilas plot close to the ideal Tschermak's substitution line (where no Fe participates in the R^{2+} of the Tschermak's substitution). Nevertheless, K white micas with Na (K-Na white micas) from Inca Huasi and San Manuel slightly deviate from the above substitution line (Fig. 3b). Iron assumed to be Fe^{3+} is the second most important octahedral cation after Al and fills less than 4 % of the octahedral site.

In regard to the parameter K p.f.u. (0.7-1.0 (t.i.c. ≥ 0.85) for ideal muscovite (Rieder *et al.* 1998) a significant variability was determined (Fig. 3c-d). Martínez *et al.* (2010) identified a clearly variable paragonite content [Na*= Na/(Na+K+Ca+Ba)] with a maximum value of ~0.45 for some dioctahedral K-Na white micas from Inca Huasi. The dioctahedral K-Na white micas of the altered basement from San Manuel display a maximum Na* of ~0.60. Besides, in the Na (a.p.f.u.) vs. K (a.p.f.u.) plot (Fig. 3c), a slight deficiency in K and Na and, thus, a deviation from the muscovite-paragonite mixing line can be recognized for all these white micas. This deviation expressed as t.i.c. value spreads out in the range of muscovite compositions (≥ 0.85), but some analyses extend to illite compositions (down to 0.80) (Fig. 3d). Pyrophyllite is a much more common mineral in the altered basement of San Manuel compared to that in the Barker area. In the outcrop at Inca Huasi (Barker), Martínez *et al.* (2010) clearly recognized pyrophyllite structure by X-ray diffractometry, the EMP analyses of which resulted occasionally in high K (0.3 a.p.f.u.) and Na (0.5 a.p.f.u.) contents. EMP analyses of pyrophyllite from San Manuel (table 1b) usually yielded discrete quantities of Na and K (Na+K < 0.32 a.p.f.u.) which scatter less compared to corresponding values for pyrophyllite from Inca Huasi (Na+K < 0.72 a.p.f.u.) (Fig. 4a). Pyrophyllite from San Manuel displays less scattered values of Si (3.50 - 3.97 a.p.f.u) and Al (2.0 - 2.5 a.p.f.u) than pyrophyllite from Inca Huasi (Si: 3.14 - 3.95 a.p.f.u.; Al: 2.04 - 2.9 a.p.f.u.). Furthermore, a negative correlation between Si (a.p.f.u) and Na+K (a.p.f.u) is less ob-

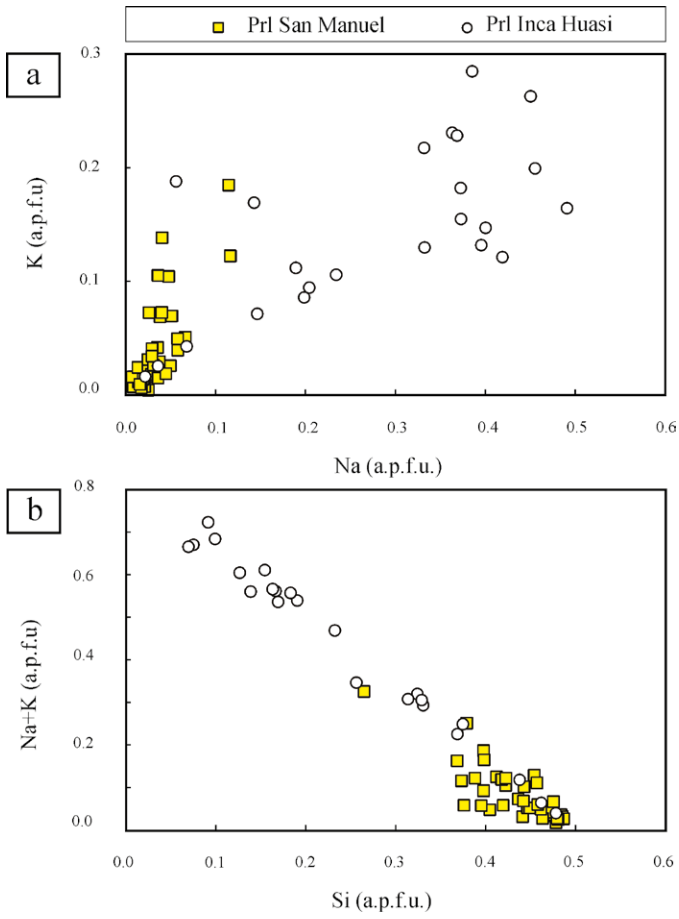

Figure 4: Compositional variation of inhomogeneous pyrophyllite analysed in samples from San Manuel and Inca Huasi (Barker).

vious for San Manuel compared to pyrophyllite from Inca Huasi (Fig. 4b). In addition, the average Si/R^3 ratio for pyrophyllite with $R^3 = Al + Fe^{3+}$ (Velde 1985) from Inca Huasi and Cerro Reconquista is 1.71 and 1.91, respectively, deviating from the theoretical, ideal ratio of 2.

Backscattered images obtained by SEM from phyllosilicates of the Inca Huasi most altered basement allow us to texturally identify different phases intergrown within K-white mica and pyrophyllite (Fig. 5). A swirl-like texture of pyrophyllite and K-white mica is a common replacement product of quartz (Figs. 5a-b). The structureless groundmass of altered rocks is dominantly composed of K-white mica and pyrophyllite (Fig. 5a) with minor amounts of APS minerals, Fe-oxide, Ti-oxide (rutile) and tourmaline. Fine intergrowths of paragonite, intermediate K-Na mica or mixed-layered K-Na-bearing micas are present in both phyllosilicates as shown in detail in figure 5c. The same textural relationship between K-white mica, pyrophyllite and K-Na mica intergrowth is observed in the groundmass of altered rocks from Inca Huasi (Figs. 5d-f). The intergrown mineral phase (paragonite, intermediate K-Na micas or mixed-layered K-Na bearing micas) can be recognized in K-white mica and pyrophyllite flakes as submicroscopic packets of wedge-shaped strips usually less than 2 μm wide, parallel to the cleavage where white micas with higher Na concentration are distinctly darker in SEM images (Fig. 5f).

P-T phase diagrams and comparison with the mineral assemblages in the studied rocks

Method

Thermodynamic modeling of P-T phase diagrams based on determined bulk-rock compositions is a very useful tool for estimating equilibrium conditions for the formation of specific mineral assemblages. The bulk-rock of the studied basement at the unconformity should be assumed to be an open system since gain and loss of elements may have occurred (Dristas *et al.* 2003; Martínez *et al.* 2010). Nevertheless, we can calculate a mineral assemblage once in equilibrium in a P-T pseudosection for most altered rocks.

By considering the chemical components of dominant mineral assemblages, bulk-rock analyses of three clue samples were modeled in the 10-component system Na-K-Fe-Mg-Mn-Al-Si-Ti-O-H with the PERPLE_X software package (Connolly 1990 - most recent version downloaded from http//www.perplex.ethz.ch on the 4th of June, 2014) for the range of 0.5-5 kbar and 150-450 ºC. Chemical analyses were simplified considering the absence of carbonate in the rocks and disregarding the presence of secondary phosphates (< 1% in vol.) (table 2). The presence of a pure hydrous fluid ($a_{H2O} = 1$) was considered to ensure complete reactions especially above 250ºC. As the phase equilibria at low temperature and intermediate pressure in hematite-rich, metasedimentary rocks were demonstrated to be highly influenced by ferric iron (e.g., Lo Pò and Braga 2014) we also evaluated the effects of different Fe^{3+} (oxygen in the bulk rock composition) contents in our rocks. Therefore, we computed P-T pseudosections with variable XFe^{3+} (Fe^{3+}/Fe_{tot}) from 0.30 to 0.65. Finally we present our results for one value of XFe^{3+} only justified by the oxidizing fluids that produced the observed mineral assemblages including hematite-goethite, which are often present in the analysed samples.

The thermodynamic data set by Holland and Powell (1998) (updated 2002) was used including the CORK equation of state for H_2O. The selected solid-solution models to reproduce the observed (most likely) mineral assemblages were: potassic white mica by Holland and Powell (1998) using a limit of the paragonite content to a molar fraction of 0.5, chlorite by Holland *et al.* (1998), biotite by Tajcmanová

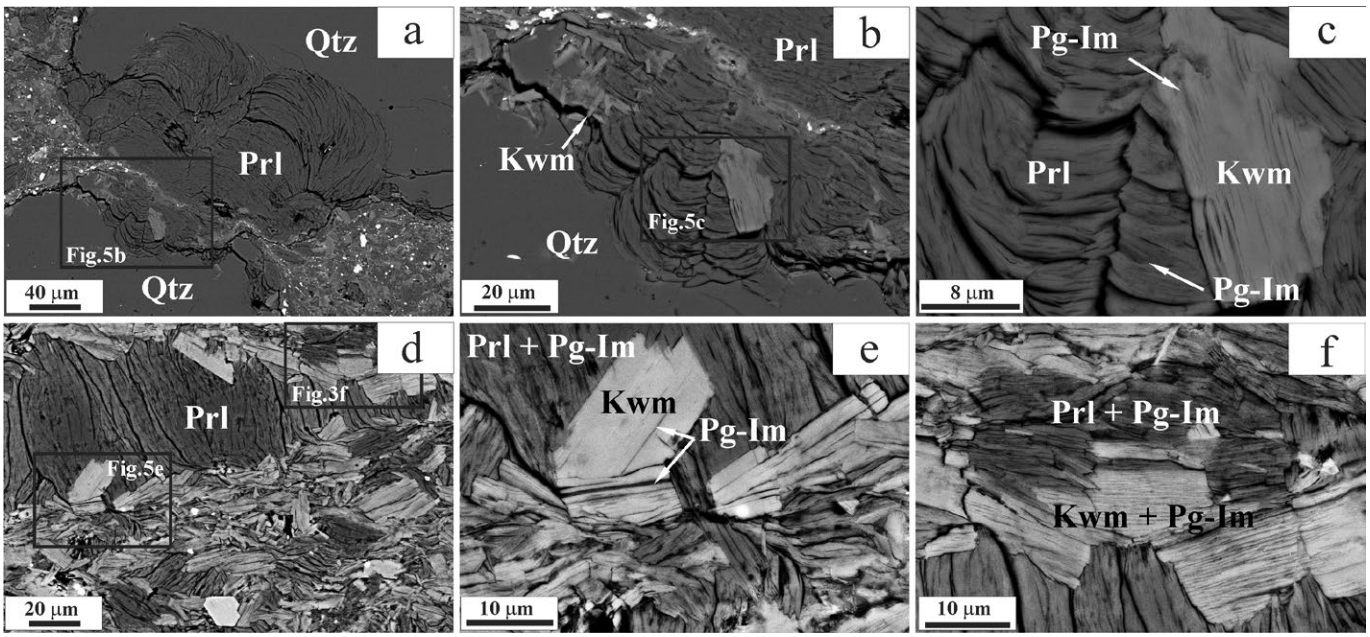

Figure 5: Backscattered SEM images of minerals in the altered migmatitic basement at the TLPU of Inca Huasi (Barker area). a) Swirl-like texture of pyrophyllite (Prl) dark-brown and K-white mica (Kwm) light-brown at the contact of two quartz (Qt) crystals. Groundmass of the alteration is seen in the lower-right and upper-left corner. b) Detail of K-white mica in pyrophyllite and quartz of the alteration matrix (upper left). c) Detail of paragonite and/or intermediate K-Na white mica (Pg-Im) in pyrophyllite and K-white mica. d) Groundmass of the alteration in an intensely replaced basement rock. e,f) Detail of coexisting pyrophyllite and K-white mica with paragonite and/or intermediate K-Na white mica.

et al. (2009), stilpnomelane by Massonne (2010), feldspar by Fuhrman and Lindsley (1988), and chloritoid by Holland and Powell (1998). Additionally, ideal ilmenite-geikielite-pyrophanite solid solution for ilmenite from the PERPLE_X data base was used. Pure end-member minerals in the calculations were andalusite, albite, diaspore, goethite, hematite, kaolinite, kyanite, magnetite, paragonite, pyrophyllite, quartz, and rutile.

The three samples (0804, 1324 and 0110) were selected according to their representative association of secondary minerals and bulk-rock chemistry. With the exception of quartz and zircon all minerals are secondary and represent more than 90 vol.% in samples from Barker (0804 and 1324) and more than 98 vol.% in the sample representative of the San Manuel area (0110), where only zircon is a remnant phase. Therefore, effective bulk-rock and true bulk-rock compositions should be (nearly) identical. The secondary minerals recognized in the evaluated samples are shown in table 3.

Thermodynamic modeling for the rock east of Cuchilla de las Aguilas: The minerals of the alteration of the basement at the TLPU from east of Cuchilla de las Águilas - La Tolva (sample 0804) (Fig. 2a and table 3) are well represented by the mineral assemblage K-white mica + chloritoid + rutile + hematite + quartz (WmCtRtHmQt) seen in the P-T pseudosections of figures 6a-b. The most likely mineral assemblage derived from the bulk rock could be well constrained for XFe^{3+} values between 0.3 (Fig. 6a) and 0.4 (Fig.6b). It is worth to mention that in the calculation with the model Pheng(HP) by Holland and Powell (1998) there is no Fe^{3+} mica end-member whereas our previous assumption for the chemical analyses was that all iron in this mica is Fe^{3+}. In both

TABLE 2: Bulk-rock composition determined by XRF (oxides in wt. %). Compositions used for PERPLE_X calculations after simplification and normalization to 100% assuming different XFe^{3+} (*, **). H_2O is saturated (sat).

Area	Barker			San Manuel					
Sample no.	0804	0804*	0804**	1324	1324*	1324**	0110	0110*	0110**
SiO_2	47.29	51.734	51.712	49.67	52.403	52.393	51.93	56.677	56.549
TiO_2	1.89	2.068	2.067	1.78	1.879	1.879	0.06	0.065	0.065
Al_2O_3	30.32	33.169	33.155	34.99	36.915	36.908	31.52	34.401	34.323
$Fe_2O_{3\,tot}$	3.86			1.25			5.92		
FeO		3.800	3.798		1.187	1.186		5.814	5.801
O_2		0.127	0.169		0.040	0.059		0.194	0.42
MnO	0.01	0.011	0.011	0.001	0.001	0.001	0.01	0.011	0.011
MgO	0.11	0.120	0.120	0.09	0.095	0.095	0.04	0.044	0.044
CaO	0.11			0.17			0.10		
Na_2O	0.28	0.306	0.306	2.33	2.458	2.458	0.84	0.917	0.915
K_2O	7.92	8.664	8.661	4.76	5.022	5.021	1.72	1.877	1.873
P_2O_5	0.68			0.18			0.09		
LOI	6.61			5.60			6.50		
H_2O		sat	sat		sat	sat		sat	sat
Sum	99.08	100.00	100.00	100.82	100.00	100.00	98.73	100.00	10.00

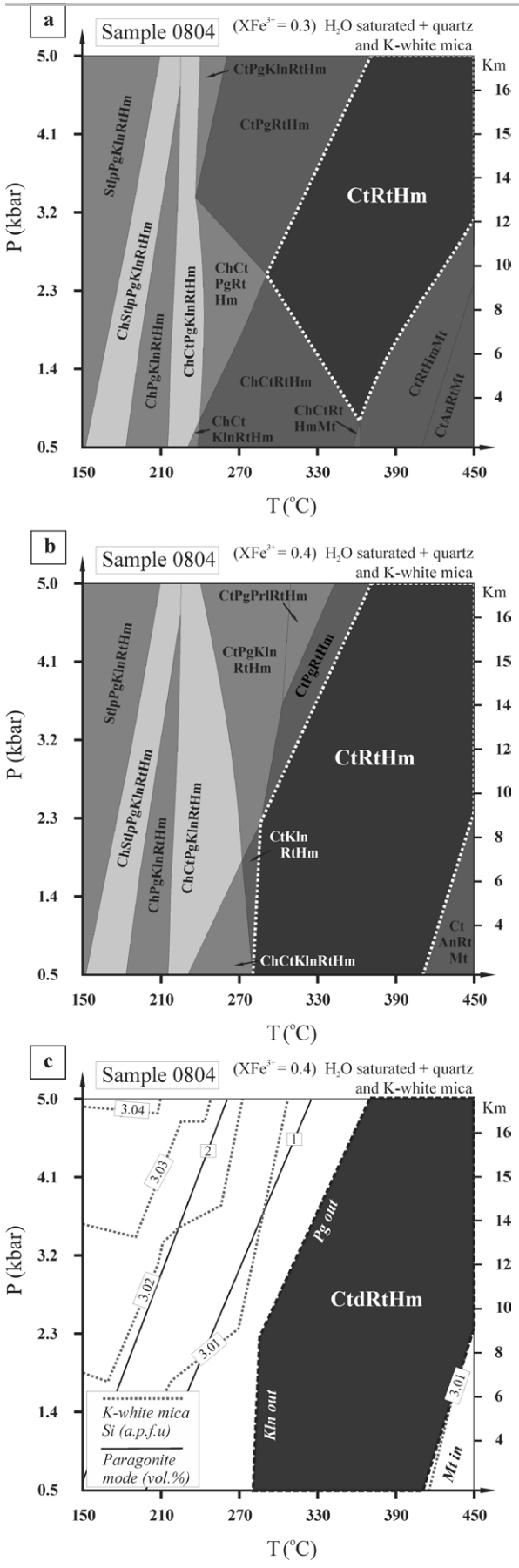

Figure 6: a, b) P-T pseudosections for the bulk-rock composition of sample 0804 (altered basement of La Tolva) calculated for XFe^{3+} = 0.3 (a) and 0.4 (b). c) Calculated modal content of paragonite and isopleths of Si (a.p.f.u.) in K-white mica for the modeled pseudosection in (b). Dashed lines limit the stability field of the observed mineral assemblage of the alteration. Abbreviations: An, andalusite; Ch, chlorite; Ctd, chloritoid; Dsp, diaspore; Goe, goethite; Hm, hematite; Kln, kaolinite; Ky, kyanite; Mt, magnetite; Pg, paragonite; Prl, pyrophyllite; Qt, quartz; Rt, rutile; Stlp, stilpnomelane; Wm, potassic white mica.

phase diagrams (XFe^{3+} = 0.3 and 0.4) the WmCtRtHmQt mineral assemblage shows a lower temperature limit at ~ 280 ºC defined by chlorite or kaolinite disappearance for XFe^{3+} = 0.3 and 0.4, respectively. For the less oxidizing system the extended stability field of chlorite reduces the most likely mineral assemblage field observed in the sample to the lowest pressure limit (Fig. 6a). In both pseudosections of the sample 0804 calculated for XFe^{3+} = 0.3 and 0.4, paragonite is not stable in the most likely mineral assemblage compatible with the finding that paragonite could not be recognized in the alteration profile of the basement from Inca Huasi neither by XRD nor by EMP studies of white micas (Martínez *et al.* 2010). In addition, the high temperature limit for WmCtRtHmQt is characterized by the appearance of magnetite which occurs at higher temperatures for the most oxidizing (XFe^{3+} = 0.4) system (Fig. 6b-c). Potassic white mica and quartz are present in the entire P-T range of the pseudosections although quartz (< 15 vol.% predicted) is only a relict (< 10 vol.%), as in Figs. 5a-b. The calculated Si content of K-white mica in the stability field of the studied mineral assemblage is around 3.01 a.p.f.u. (shown for XFe^{3+} = 0.4 in figure 6c). EMP data yielded a slightly variable range between 3.02-3.10 a.p.f.u, analytical errors not considered. Rutile and hematite are accessories in the mineral assemblage.

Thermodynamic modeling for the Inca Huasi sample: Sample 1324 was surveyed at the TLPU close to the Inca Huasi ranch, NE Barker area (Fig. 2a). The stability field of the mineral assemblage K-white mica + chloritoid + paragonite + pyrophyllite + rutile + hematite + quartz (WmCtPgPrlRtHmQt) could be assigned to the secondary minerals identified in the sample (table 3). According to calculations for XFe^{3+} between 0.3 (Fig. 7a) and 0.45 (Fig. 7b), this mineral assemblage defines a narrow temperature field, which is limited at low pressures (< 2 kbar) in the modeled pseudosections (Figs. 7a-b) by the presence of chlorite below 330 - 340 ºC and the breakdown of pyrophyl-

lite at 340 ºC (1 kbar = ~ 4 km) - 370 ºC (2.3 kbar) to andalusite. At values higher than 0.45 of XFe^{3+} the field of WmCtPgPrlRtHmQt is strongly shrunken to higher pressures and temperatures until it disappears with rising XFe^{3+}. Kaolinite, identified in this sample with a mode of < 5 vol. % is stable at temperatures < 280 ºC. Quartz, which occurs in the entire P-T pseudosection together with secondary K-white mica grains, is relatively scarce in the rock (7-8 vol. %). High contents of paragonite (24 to 26 vol.%), as an individual mineral phase, were calculated (Fig. 7c).

Thermodynamic modeling for the rock at San Manuel: The altered basement from the San Manuel area at ~3m below the unconformity, represented by sample 0110 (Cantoni quarry, figure 2b), is composed of pervasive replacement products of fine grained (< 50 μm) pyrophyllite, K-white mica, kaolinite (< 10 vol.%), hematite-goethite (15-18 vol.%), and clusters of idiomorphic diaspore crystals (8 - 10 vol.%) (table 3). Accessory minerals such as prismatic crystals of tourmaline (< 4 vol.%), rutile (< 2 vol.%) and clusters of tiny APS minerals (< 1 vol.%) are widespread. In the P-T pseudosections calculated for sample 0110 the observed minerals can be recognized in the unique field K-white mica + chloritoid + paragonite + pyrophyllite + rutile + hematite + diaspore (WmCtPgPrlRtHmDsp) above 280ºC. Quartz is absent at very low pressure and very low temperature in the calculated phase diagram when diaspore is present. For the assemblage WmCtPgPrlRtHmDsp a wide range of oxidizing conditions is possible since virtually no changes were observed from 0.3 to 0.65 XFe^{3+} (Figs. 8a-b). Compared to the pseudosections for sample 1324 (Inca Huasi) the breakdown of pyrophyllite to form kyanite or andalusite occurs for sample 0110 (Fig. 8a-b) already at temperatures of ≥330 ºC. Likewise, kaolinite recognized in XRD spectra and in BSE images, as alternative to pyrophyllite, is stable up to 280 ºC and does not belong to the WmCtPgPrlRtHmDsp assemblage observed in sample 0110 (table 3). The calculated modal content of pyrophyllite and K-white mica is 45 % and 15 %, respectively, in agreement with the proportions estimated from BSE images. According to the thermodynamic modeling K-white mica is a nearly pure phase hardly mixing with paragonite. The calculated content of paragonite for the most oxidizing conditions is close to 10 vol.% (Fig. 8c). The real low proportion of paragonite (< 5 vol.%) in this sample hampers its identification in X-ray diffractograms (table 3).

TABLE 3: Mineral assemblages and other minerals identified *(in italics)* by optical microscopy and/or by X-ray diffractometry.

Sample	Mineral assemblage and others minerals	Locality
0804	K-white mica + hematite-goethite + rutile + tourmaline + APS minerals *(relictic quartz and zircon).*	La Tolva (Cuchilla de las Aguilas)
1324	Pyrophyllite + K-white mica + paragonite/intermediate K-Na mica + hematite-goethite + rutile + APS minerals + tourmaline ± *kaolinite (relictic quartz and zircon).*	Inca Huasi
0110	Pyrophyllite + K-white mica + goethite-hematite + diaspore + rutile + tourmaline + APS minerals ± *kaolinite (relictic zircon).*	Cerro Reconquista (Cantoni quarry)

$^{40}Ar/^{39}Ar$ thermochronology

Sample 0420, representative of the altered basement from the San Manuel; is located ~ 8 m below the unconformity, from east of Verellén quarry (Fig. 2b). According to XRD spectra, it is composed of muscovite (2M1-1M) + pyrophyllite + hematite-goethite + quartz. The Ar degassing pattern of this sample, suggestive of excess of argon, gave a total gas age of 660 ± 30 Ma (table 4a). Ar excess is confirmed by the "reverse isochron" plot (not shown) which indicates an initially trapped argon composition well in excess of $^{40}Ar/^{36}Ar$ = 295.5. Ages were recalculated using the trapped component of 6000 ± 3000, indicated by the reverse isochron, and omitting the first two steps, which were likely dominated by a more normal atmospheric trapped component. Then the sample yields a spectrum with an integrated age (n = 12) of 620 ± 30 Ma and a well defined plateau age (n = 6) of 630 ± 30 Ma (Fig. 9 and tables 4a and b).

DISCUSSION

Compositions of K-white mica and pyrophyllite in the altered rocks

The somewhat variable chemical compositions in K and Na contents of K-white micas in the altered basement at the TLPU cannot be explained solely by common cation substitutions in white micas at low temperatures (Rieder *et al.* 1998). And therefore, we assume that submicroscopic inhomogeneities detected on SEM images (Figs. 5a-f) are responsible for mixed K-Na white mica analyses. K-white micas from the east of Cuchilla de la Aguilas (La Tolva and Cerro del Medio profiles) display mineral compositions approaching that of ideal muscovite (Fig. 3a). In contrast, comparable K-Na white micas from Inca Huasi and San Manuel show higher contents of Si and Na. The aforementioned deviation from the Tschermak´s substitution line (Fig. 3b) and the muscovite-paragonite mixing line (Fig. 3c) could be well explained by the pyrophyllitic substitution (^{XII}(Na, K) ^{IV}Al = $^{XII}\square$ ^{IV}Si). Such kind of substitution is well known in low grade (LT-LP) metamorphic rocks (e.g. Agard *et al.* 2001; Parra *et al.* 2002). Moreover, the broader extension of this substitution in samples from Inca Huasi and San Manuel is coincident with the existence of pyrophyllite as an individual mineral phase. In addition, values of Si as high as 3.2 a.p.f.u. (Fig. 3b) may possibly result from quartz contamination, although there is little in the altered rocks, when analyzing very small mica laths (< 4 μm). Abad *et al.* (2006) evaluated the possible analytical artefacts affecting the quality of chemical data in very fine-grained dioctahedral white micas. According to these authors, interference caused by quartz contamination result in a drop in the interlayer cation content coupled with an increase in silica content. As we not-

TABLE 4a: Detail of the $^{40}Ar/^{39}Ar$ analytical results of step-heating thermochronology from a sample of the altered basement from San Manuel.

Sample 0420									J-factor	J error
Step ID	Temp	$^{40}Ar/^{39}Ar$	$^{37}Ar/^{39}Ar$	$^{36}Ar/^{39}Ar$ (x10^{-3})	39ArK (10^{-16} mol)	K/Ca	$^{40}Ar^{*}$ (%)	^{39}Ar (%)	Age (Ma)	± 1σ (Ma)
A	300	127.672	4.0960	0.0948	0.2685	0.12	78.3	2.1	220.0	6.01
B	400	249.093	1.6708	0.0242	0.7419	0.31	97.2	5.8	491.9	2.19
C	450	379.300	0.6318	0.0130	1.2032	0.81	99.0	9.4	714.4	1.36
D	500	381.239	0.2883	0.0092	1.4458	1.77	99.3	11.3	719.0	1.17
E	550	368.277	0.3542	0.0092	1.7881	1.44	99.3	14.0	698.6	1.12
F	600	353.227	0.3935	0.0060	1.9907	1.30	99.5	15.6	676.2	1.19
G	650	344.420	0.2670	0.0040	1.7898	1.91	99.7	14.0	662.9	0.75
H	700	340.140	0.2566	0.0039	1.4332	1.99	99.7	11.2	656.0	1.11
I	750	341.561	0.4301	0.0017	0.8822	1.19	99.9	6.9	659.4	1.12
J	800	338.889	0.2973	0.0060	0.4839	1.72	99.5	3.8	653.0	1.40
K	850	345.868	0.1589	0.0105	0.3117	3.21	99.1	2.4	662.1	2.58
L	900	341.545	0.1124	0.0089	0.2071	4.54	99.2	1.6	655.8	2.24
M	950	359.072	0.3531	0.0291	0.1496	1.45	97.6	1.2	674.6	4.09
N	1000	351.913	0.7030	0.0320	0.0504	0.73	97.3	0.4	661.9	8.31
O	1050	399.220	14.9091	0.2808	0.0131	0.03	79.5	0.1	626.1	34.23
Total gas age plateau				**n= 15**	**12.76**	**Steps A-O**		**100.00**	**660.0**	**30**

Note. Isotopic ratios corrected for blank, radioactive decay, mass discrimination, and interfering reactions.
Individual analyses show analytical error only; plateau and total gas age errors include error in J and irradiation parameters.
Analyses in italics are excluded from the plateau age calculations.
n= number of heating steps.
K/Ca = molar ratio calculated from reactor produced ^{39}ArK and $^{37}ArCa$.

TABLE 4b: Continued from 4a.

Sample 0420									J-factor	J error
Step ID	Temp	$^{40}Ar/^{39}Ar$	$^{37}Ar/^{39}Ar$	$^{36}Ar/^{39}Ar$ (x10^{-3})	39ArK (10^{-16} mol)	K/Ca	$^{40}Ar^{*}$ (%)	^{39}Ar (%)	Age (Ma)	± 1σ (Ma)
C	450	379.300	0.6318	0.0130	1.2032	0.81	80.0	10.3	597.2	8.40
D	500	381.239	0.2883	0.0092	1.4458	1.77	85.9	12.3	637.0	5.47
E	550	368.277	0.3542	0.0092	1.7881	1.44	85.3	15.2	615.3	6.92
F	600	353.227	0.3935	0.0060	1.9907	1.30	90.1	17.0	622.3	5.44
G	650	344.420	0.2670	0.0040	1.7898	1.91	93.2	15.3	626.4	5.08
H	700	340.140	0.2566	0.0039	1.4332	1.99	93.2	12.2	620.2	5.84
I	750	341.561	0.4301	0.0017	0.8822	1.19	97.2	7.5	644.6	7.96
J	800	338.889	0.2973	0.0060	0.4839	1.72	89.7	4.1	598.3	13.03
K	850	345.868	0.1589	0.0105	0.3117	3.21	82.0	2.7	564.0	21.66
L	900	341.545	0.1124	0.0089	0.2071	4.54	84.5	1.8	572.5	32.38
M	950	359.072	0.3531	0.0291	0.1496	1.45	52.0	1.3	390.7	59.12
N	1000	351.913	0.7030	0.0320	0.0504	0.73	46.4	0.4	345.8	123.44
Total gas age plateau		**MSWD= 2.67**		**n= 12**	**11.74**	**Steps C-N**		**100.00**	**620.0**	**30.0**
				n= 6	**9.33**	**Steps D-I**	**79.50**	**630.0**	**30.0**	

Note. Isotopic ratios corrected for blank, radioactive decay, mass discrimination, and interfering reactions.
Individual analyses show analytical error only; plateau and total gas age errors include error in J and irradiation parameters.
Analyses in italics are excluded from the plateau age calculations.
n= number of heating steps.
K/Ca = molar ratio calculated from reactor produced ^{39}ArK and $^{37}ArCa$.

ed only a very slight tendency of t.i.c. decrease with Si increase (enhanced in figure 3d by the ratio Si/Al), we conclude that such Si increase is more likely caused by the previously mentioned pyrophyllitic substitution. Likewise, the analytical artefact of alkali cation loss in K-dioctahedral micas during chemical analyses could be suggested by a decrease of the interlayer cation content together with an apparent increase of Si and Al (Abad *et al.* 2006). As this correlation of decreasing t.i.c. with increasing Al is not seen in the chemistry of our micas we discard alkali-loss during the performance of our analyses.

Another substitution that was recognized in the studied micas is the ferrimuscovite substitution ($Al^{VI, IV} = Fe^{3+}$) (Martínez *et al.* 2010) despite low iron contents (Fe^{3+}) in the octahedral site (<

4%). In any case, such a low amount of total iron content would minimize the uncertainties of considering all iron in micas as Fe^{3+}, whereas the solution model Pheng(HP) uses only Fe^{2+}.

According to Jiang and Peacor (1993), apparent compositions intermediate between paragonite and muscovite (at low temperatures) may have three possible origins: (1) averaging of very-fine scale intergrowths of paragonite with muscovite, (2) averaging of mixed-layered paragonite-muscovite, or (3) homogeneous metastable solid-solution members. The first two possibilities require paragonite or mixed-layered paragonite-muscovite formation. Our thermodynamic modeling with PERPLE_X shows that at H_2O saturation and relatively high oxidation (considerable Fe^{3+} contents) various bulk-rocks can be suitable protoliths for the formation of paragonite, muscovite, pyrophyllite and other addressed minerals at specific pressure and low temperature (T > 280 °C) conditions. In open systems such as hydrothermal environments, steady states of equilibrium (or local equilibrium) may be reached. Thus, metastable Na- and K-bearing micas can be only intermediate products due to incomplete transformation of a preexisting mineral to paragonite and muscovite at temperatures where micas close to end-member composition form according to known solvus relations (Guidotti *et al.* 1994). Summarizing our results, WDS analyses (Figs. 3-4) and SEM imagery (Fig. 5) allowed us to prove the existence of K-Na phyllosilicates intergrown either in dioctahedral K-white mica and pyrophyllite, but the spatial resolution of the applied methods precludes the recognition of regular mixed-layering or possible homogeneous metastable solid-solution phases between end-members paragonite, muscovite, and pyrophyllite in the nanometre range. Therefore, variable compositions determined for K-white micas in several alteration profiles at the two study areas, with maximum values of $Ms_{55}Pg_{45}$ and $Ms_{40}Pg_{60}$, plotting outside the muscovite-paragonite binary solvus, cannot be considered as composition of intermediate

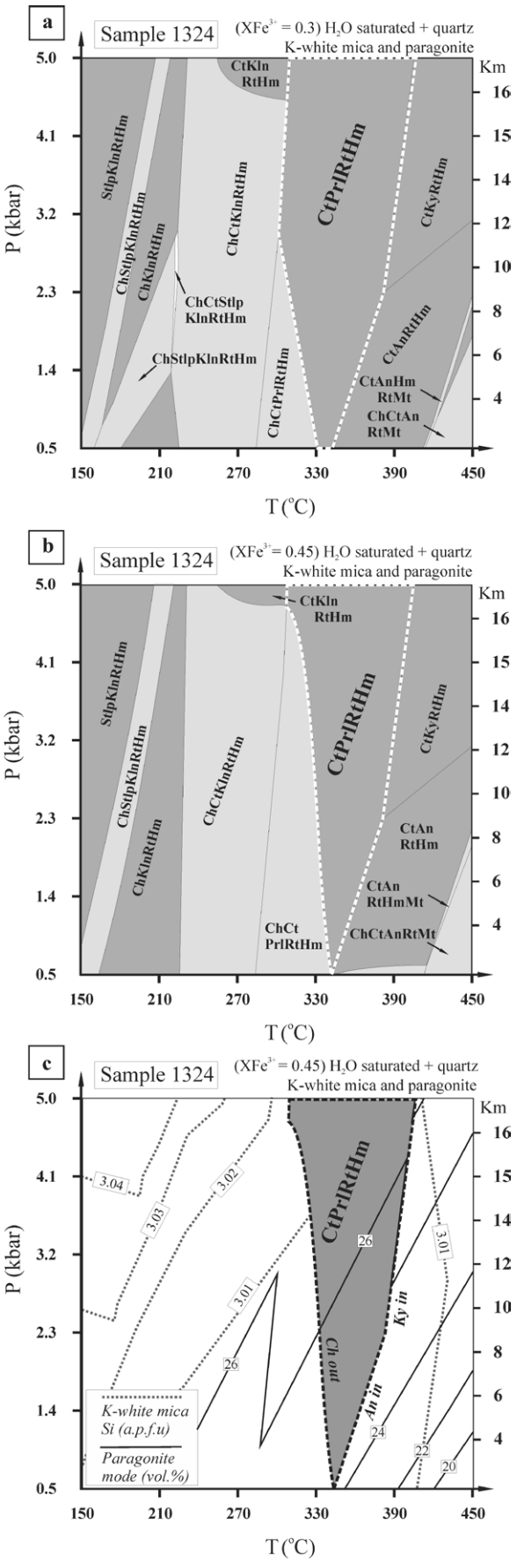

Figure 7: a, b) P-T pseudosections for the bulk-rock composition of sample 1324 (altered basement of Inca Huasi) calculated for XFe^{3+} = 0.3 (a) and 0.45 (b). c) Calculated modal content of paragonite and isopleths of Si (a.p.f.u.) in K-white mica for the modeled pseudosection in (b). Dashed lines limit the stability field of the observed mineral assemblage of the alteration. Abbreviations as in figure 6.

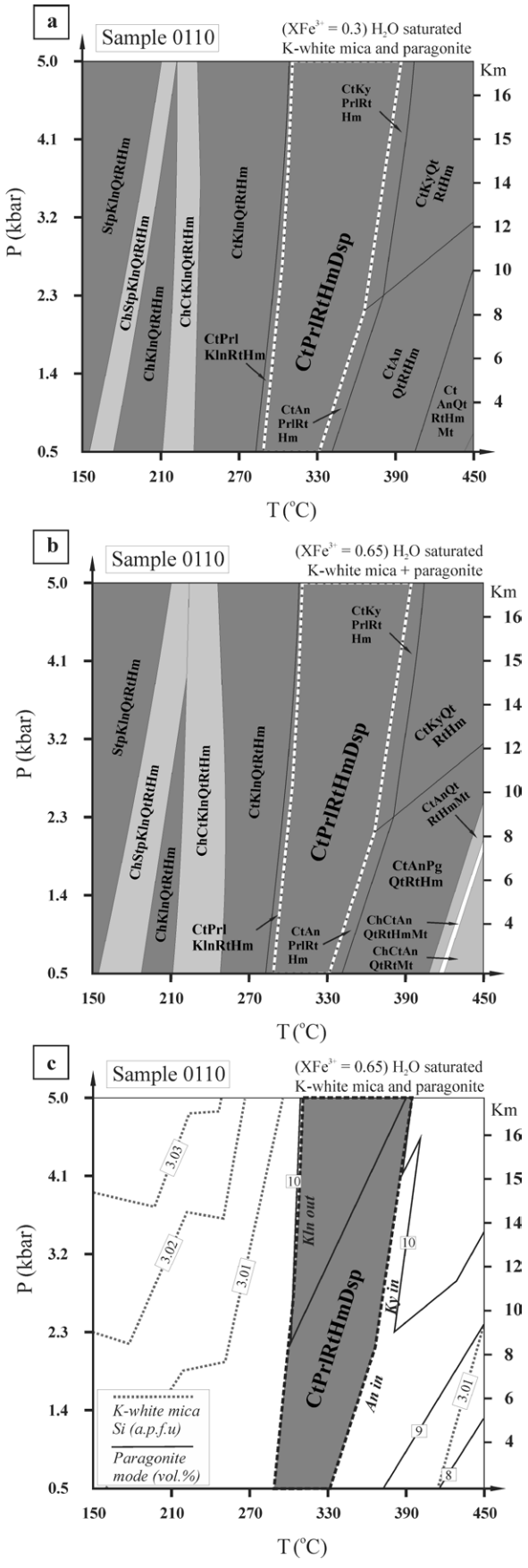

Figure 8: a, b) P-T pseudosections for the bulk-rock composition of sample 0110 (altered basement of San Manuel) calculated for XFe^{+3} = 0.3 (a) and 0.65 (b). c) Calculated modal content of paragonite and isopleths of Si (a.p.f.u.) in K-white mica for the modeled pseudosection in (b). Dashed lines limit the stability field of the observed mineral assemblage of the alteration. Abbreviations as in figure 6.

phases until a survey at a suitable scale, using AEM and TEM, were achieved.

The same must be argued for variable contents of Na and K in pyrophyllite from both localities, Barker and San Manuel. The presence of K-Na-bearing mica (Fig. 4a) in the excitation volume of the electron beam of the EMP has an effect on the amount of SiO_2 of pyrophyllite. We noted a negative correlation between Na+K and SiO_2 pointing to phase inhomogeneities (Fig. 4b) as observed in SEM images. As a consequence, the Si/R^3 ratio is lower than the ideal value of 2 (table 1b). Similarly, chemical analyses of natural pyrophyllites with Na and K contents were reported (Newman and Brown 1987; Lackschewitz *et al.* 2004) and such chemical variation is more likely due to interstratifications (e.g. Jiang *et al.* 1990; Ruiz Cruz *et al.* 2004). A better constraint was presented by Martínez *et al.* (2010) who confirmed the existence of basal reflections of 1M muscovite, 2M1 muscovite and pyrophyllite as well as discrete quantities of regular interlayering of paragonite and an intermediate K-Na mica in the most altered basement of Inca Huasi (Barker area) by means of X-ray diffractometry.

Árkai *et al.* (2008) emphasized the influence of the bulk-rock composition on the fluid chemistry by the formation of paragonite and/or precursor minerals in very low-grade metaclastic rocks. At the studied unconformity (TLPU) the most widespread igneous-metamorphic basement rocks, gneisses and migmatites (Dristas *et al.* 2003; Dristas and Martínez 2007; Martínez and Dristas 2007; Martínez *et al.* 2010), contain variable proportions of plagioclase (andesine) (< 40 vol.%), biotite (< 30 vol.%) and K-feldspar (< 30 vol.%). Therefore, sodium and potassium were regionally easily available in the protoliths of secondary mineral alterations. These igneous and high-grade metamorphic basement rocks themselves behaved inert to the formation of paragonite. But textural and chemical transformations (leaching) of basement rocks occurred at the TLPU by metasomatism (e.g., Dristas *et al.* 2003; Dristas

and Martínez 2007; Martínez and Dristas 2007; Martínez *et al.* 2010; Fernández *et al.* 2010) and/or palaeoweathering (Zalba *et al.* 1992; Fernández *et al.* 2010) resulting in effective bulk-rock compositions which have favoured, for instance, the formation of paragonite at relatively low temperatures. Thus, the presence of paragonite in the studied rocks can be best explained by Na mobilization during hydrothermal alteration of basement rocks. The influence of the chemistry of the protolith on the occurrence of paragonite in metamorphic rocks was early recognized by Baltatzis and Wood (1977). According to the aforementioned authors, the compositional parameter that is likely to be of greatest effect for the formation of paragonite is the Al content of the rocks apart from their Na/(Na+K) ratio. Hydrolysis of feldspar in the most altered basement rocks at the TLPU has generated Al-rich products. Thus, in our case it is not necessary to carry alumina by hydrothermal fluids from long distances as were stated, for instance, for the British Lower Palaeozoic metaclastic mudrocks in an extensional setting (Merriman 2006). In some samples of the altered sedimentary rocks immediate to the contact (sample 1025- north of Sierra de la Juanita and 1324 from Inca Huasi) Na and K would be also available from alteration of clastic feldspars in the overlying sediments. Indeed, such feldspars can be completely replaced by clay minerals. Hence, dissolution and crystallization seems to be the most striking processes in the formation of K-Na bearing micas driven by the presence of hydrous fluids, as it is commonly stated for low temperature hydrothermal alteration of phyllosilicates (Shau *et al.* 1991; Jiang and Peacor 1993).

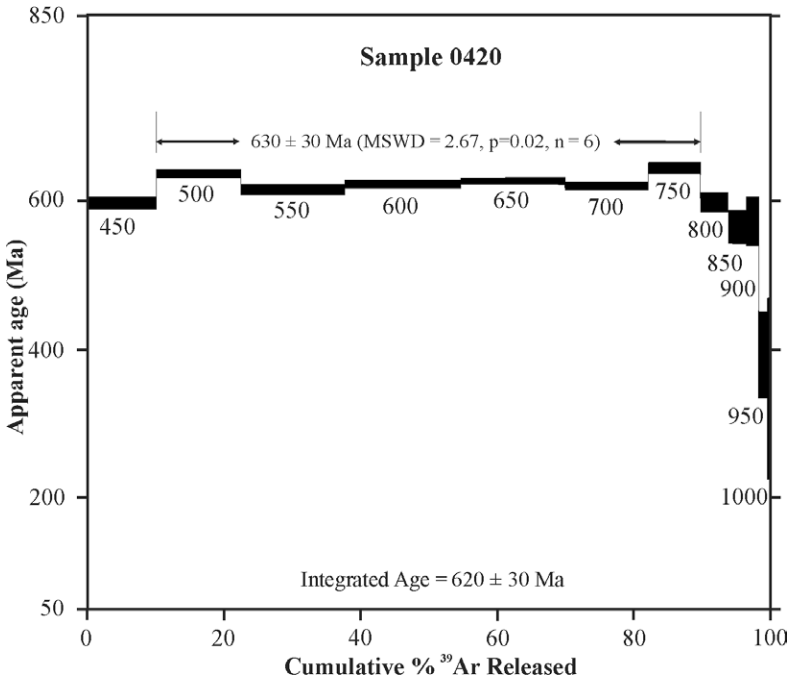

Figure 9: Ar degassing pattern obtained by step-heating of K-white mica rich sample 0420 from the altered basement of San Manuel (eastern Verellén quarry).

P-T conditions of the alteration in the studied rocks

The P-T pseudosections of figures 6-8 indicate that under H_2O saturated and variable oxidizing conditions, most of the observed secondary minerals represent assemblages formed at temperatures > 280 °C. Furthermore, these mineral assemblages are relatively insensitive to pressure changes, under the studied condition ranging from 0.5 to 5 kbar, with the exception of sample 0804 (La Tolva) for the condition of $XFe^{3+} = 0.3$. In this case the studied mineral assemblage is stable above ~0.7 kbar (~3 km) (Fig. 6a). Martínez *et al.* (2013) established similar minimum temperatures of formation (~300 ºC) using the illite crystallinity of secondary K-white micas of the basement alteration at the unconformity from east of Cuchilla de las Aguilas (La Tolva). Microthermometry of secondary fluid inclusions in relictic quartz crystals of the altered basement at Cerro Reconquista (San Manuel area) yielded two populations of trapping temperatures: 180-190ºC and 300-320ºC (Dristas and Frisicale 1984). The range of higher trapping temperatures is in accordance with the calculated P-T field of the observed mineral assemblage (Fig. 8a-c).

The lower sedimentary unit overlying the altered basement in the Barker area was estimated to be buried to less than 4 km (~1 kbar) (Alló *et al.* 2000; Zalba *et al.* 2007). Besides, in the Olavarría area (50 km northwards from Barker, figure 1), the same lowermost sedimentary unit reached a very deep mesodiagenetic stage: ~200 ºC and 5-6 km (< 1.5 kbar) (Gómez Peral *et al.* 2011). According to Martínez *et al.* (2013), an illite crystallinity indicative of anchizonal realms with temperatures of 300 to 350 °C was determined for the altered basement from La Tolva. Besides, these authors indicated that for a normal geothermal gradient such anchizonal conditions can be correlated with unexpected depths of more than 9.5 km of overburden. This incongruence was explained by the migration of hot fluids through the unconformity after diagenesis of the overlying sedimentary pile.

In addition to the calculated mineral assemblages, the studied samples may contain accessory secondary minerals such as tourmaline and APS minerals that were not modeled. But the occurrence of kaolinite in samples from Inca Huasi (1324) and San Manuel (0110) which do not belong to the peak-temperature mineral assemblages can be either explained as a result of incomplete reactions to form pyrophyllite (+ diaspore) or, more likely, as a late alteration phase generated during waning temperatures of penetrat-

ing hydrothermal fluids. Correspondingly, Fernández *et al.* (2010) uttered a meteoric origin for kaolinite.

Moreover, the appearance of chloritoid in the calculated peak-temperature mineral assemblage, but not found in any of the studied samples, cannot satisfactorily be explained. Chloritoid is a mineral phase well known in very low grade metamorphic rocks with a common mineral assemblage such as those mentioned above (e.g. Zen 1960; Frey 1978; Livi *et al.* 1997; Árkai *et al.* 2008). For our samples, maximum contents of chloritoid of 2 vol.% (sample 1324), 7 vol.% (sample 0804) and 12 vol.% (sample 0110) were calculated for temperatures above 210 °C. However, the cations in this mineral phase, namely Fe^{2+}, Mg^{2+} and Mn^{2+}, could have been consumed for the formation of tourmaline in the three modeled samples as the boron contents were not considered in the PERPLE_X calculations. This tourmaline, with maximum contents of 3 vol.% in these samples, forms secondary needle-like prismatic crystals (Dristas and Frisicale 1984; Martínez and Dristas 2007) which can be easily distinguished from relictic thick columns of pegmatitic-metamorphic tourmaline such as those seen in samples from Cerro Reconquista. The thermodynamic calculations for higher oxidizing conditions do not offer an alternative for the absence of chloritoid. A further explanation is the possibility of the transformation of pre-existing chloritoid to kaolinite (+ oxides) by hydrothermalism after the most pervasive fluid-related alteration at waning temperatures < 200 °C. Once again, the hypothesis of later hydrothermal fluids with lower temperatures could well explain, for instance the formation of kaolinite, in agreement with late fluid inclusions (Dristas and Frisicale 1984) and younging of K/Ar ages of alteration in the upper sedimentary succession (Martínez *et al.* 2013).

Age of alteration

Sample 0804 modeled in the P-T pseudosection of figures 6a-b corresponds to a phyllic alteration of the basement east of Cuchilla de las Aguilas - La Tolva (Barker) dominated by muscovite (2M1-1M). This altered basement yielded a bulk-rock K/Ar age of 616 ± 17 Ma (Dristas and Martínez 2007) and a K/Ar age on fine fractions of 587.7 ± 6.2 - 572.5 ± 6.9 Ma (Martínez *et al.* 2013). The methodology of dating fine-grained fractions (< 2 μm) of K-white micas would certainly constrain the age of any younger event and could be linked to one of the muscovite polytypes such as 1M. Therefore, these ages are compatible or at least in the proximity with the here determined $^{40}Ar/^{39}Ar$ age plateau of 630 ± 30 Ma for the phyllic alteration of the basement of Cerro Reconquista (San Manuel). The studied samples of altered basement from both sectors (Barker and San Manuel) have experienced minimum temperatures of formation of > 280 °C.

The low-grade meta-siltstones of the Punta Mogotes Formation (Marchese and Di Paola 1975), only recognized in drill holes at 130 km SE of the Barker area near Mar del Plata (Fig. 1), gave four K-Ar ages, dating the last thermotectonic event between 576 ± 13 Ma and 615 ± 14 Ma (Cingolani and Bonhomme 1982). The ages related to the alteration at the unconformity are in accordance with vertical tectonic movements, block faulting with basement uplift, during the Brasiliano orogenic cycle around 600 Ma (Iñiguez-Rodriguez *et al.* 1989). Hence, Martínez *et al.* (2013) delimited the age of the hydrothermal activity from the data set of K/Ar ages on fine fractions of the altered basement from Barker and K/Ar ages of alunite from the middle stratigraphic level of the overlying sedimentary succession between *ca.* 620-590. This wide age range could be due to the penetration of hydrothermal fluids over a long period of time or the impossibility to reliably date several low-temperature events followed by periods of non-interacting fluids. But in any case, the various ages of alteration are clearly younger than Cryogenian (~ 800 Ma) ages of sedimentation/diagenesis of the basement overlying lower sedimentary unit (Villa Mónica Formation).

CONCLUSIONS

Paragonite and intermediate K-Na white mica (?) are locally present as interlayer phases within K-white mica and pyrophyllite of the most pervasively altered basement at the TLPU in a widespread area (>50 km). The hydrothermal alteration of basement rocks led to dissolution of precursor minerals, such as feldspars, and crystallization of K-Na bearing micas among other phyllosilicates. The identification of limited chemical variations in K-white mica, as expected in this relatively low temperature hydrothermal-metamorphic realm, is complicated by interlayered Na-bearing micas. In chemical variation in pyrophyllite is only possible by paragonite and/or intermediate K-Na white mica intergrowths. The mineral assemblages in P-T pseudosections, thermodynamically calculated with PERPLE_X, show that the minimum temperature for the formation of the studied alteration was 280 °C at oxidizing conditions ($XFe^{3+} > 0.3$). Above this temperature for a wide and variable range of higher temperatures different phyllosilicate assemblages formed in the most pervasively altered basement. The occurrence of paragonite in these assemblages strongly depends on the bulk-rock composition (protolith) as suggested in previous works. As a conclusive result, the P-T pseudosection modeling was capable to define a temperature range at which the observed secondary minerals (either their intergrowths) were once in equilibrium and therefore formed at the same time. But the modeling also supports the hypothesis that minerals such as kaolinite would have formed at waning temperatures of the same event or by another younger event of lower temperatures. In addition, the ages of formation of the K-white micas (either 2M1 and/or 1M) and its associated mineral assemblage point to a hydrothermal activity, responsible for the basement alteration, lasting over a long period of time from ca. 630 Ma to 590 Ma, eventually with interruptions. In any case, the hydrothermal fluid flow event can be related to block movements during the diachronic late Neoproterozoic Brasiliano orogenic cycle.

ACKNOWLEDGEMENTS

We are grateful to the institutions Agencia Nacional de Promoción Científica y Tecnológica (ANPCYT) (J.A.D., PICT 2010 N° 949), Alexander von Humboldt Foundation (H-J.M., 3.4 -Fokoop_ ARG/1005880), and Deutscher Akademischer Austauschdienst (A/07/97229) for granting short-stay fellowship at the Institut für Mineralogie und Kristallchemie, Universität Stuttgart, to J.C.M. We thank Thomas Theye (Universität Stuttgart) and Rolf Neuser (Ruhr-Universität Bochum) for their valuable assistance in EMP and SEM data survey. The authors are also indebted to reviewers Fernanda Cravero and Gilda Collo who made valuable suggestions for its improvement.

REFERENCES

Abad I., Nieto, F., Gutiérrez-Alonso, G., Do Campo, M. López-Munguira A. and Velilla, N. 2006. Illitic substitution in micas of very low-grade metamorphic clastic rocks. European Journal of Mineralogy, 18: 59-69.

Agard, P., Vidal, O., Goffé, B. 2001. Interlayer and Si content of phengite in HP-LT carpholite-bearing metapelites. Journal of Metamorphic Geology, 19: 477-493.

Alló, W.A., Domínguez, E.A. and Cravero, F. 2000. Calidad de las arcillas precámbricas de las facies silicoclásticas de la Formación Villa Mónica en el área de Barker, provincia de Buenos Aires, Argentina. 2° Congreso Latinoamericano de Sedimentología y 8° Reunión Argentina de Sedimentología, 30-31, Mar del Plata, Argentina.

Árkai, P., Faryad, S.W., Vidal, O. and Kadosa, B. 2003. Very low-grade metamorphism of sedimentary rocks of the Meliata unit, Western Carpathians, Slovakia: implications of phyllosilicate characteristics. International Journal of Earth Sciences (Geologische Rundschau), 92: 68-85.

Árkai, P., Livi, K.J.T. and Horváth, P. 2008. Dioctahedral mixed K-Na-micas and paragonite in diagenetic to low-temperature metamorphic terrains: bulk-rock chemical, thermodynamic and textural constraints. Central European Geology, 54 (4): 283-314.

Baltatzis, E. and Wood, B.J. 1977. The occurrence of paragonite in chloritoid schist from Stonehaven, Scotland. Mineralogical Magazine, 41: 211-216.

Cingolani, C.A. and Bonhomme, M.G. 1982. Geochronology of La Tinta Upper Proterozoic sedimentary rocks, Argentina. Precambrian Research, 18: 119-122.

Cingolani, C.A. and Bonhomme, M.G. 1988. Resultados geocronológicos en niveles peliticos intercalados en las dolomías de Sierra Bayas (Grupo La Tinta), provincia de Buenos Aires. Segundas Jornadas Geológicas Bonaerenses, Actas: 283-289, Bahía Blanca.

Cingolani, C.A. and Dalla Salda, L. 2000. Buenos Aires cratonic region. In Cordani, U.G., Milani, E.J,. Filho, A.T and Campos, D.A. (eds.) Tectonic Evolution of South America, 21° International Geological Congress, 139-147, Rio de Janeiro, Brazil.

Cingolani, C.A., Hartmann, L.A., Santos, J.O., McNaughton, N.J. 2002. U-Pb SHRIMP dating of the zircons from the Buenos Aires Complex of the Tandilia Belt, Río de la Plata Craton, Argentina. 15° Congreso Geológico Argentino, Actas 1: 149-154, El Calafate.

Cingolani, C.A., Santos, J.O.S., McNaughton, N.J., Hartmann, L.A. 2005. Geocronología U-Pb SHRIMP sobre circones del granitoide Montecristo, Tandil, provincia de Buenos Aires, Argentina. 16° Congreso Geológico Argentino, Actas 1: 299-302, La Plata.

Connolly, J.A.D. 1990. Multivariable phase diagrams; an algorithm based on generalized thermodynamics. American Journal of Science, 290: 666-718.

Dalla Salda, L. and Iñiguez-Rodriguez, A.M. 1979. La Tinta, Precámbrico y Paleozoico de Buenos Aires. 7° Congreso Geológico Argentino, Acta 1: 539-550, Neuquén.

Deino, A.L. 2001. Users manual for Mass Spec v. 5.02. Berkeley Geochronology Center, Special Publication, 1a, 119 p., Berkeley.

Dristas, J.A. and Frisicale, M.C. 1984. Estudio del yacimiento de arcilla del cerro Reconquista, San Manuel, Sierras Septentrionales de la provincia de Buenos Aires. 9° Congreso Geológico Argentino, Actas 5: 507-521, San Carlos de Bariloche.

Dristas, J.A., Frisicale, M.C. and Martínez, J.C. 2003. High-REE APS minerals associated with advanced argillic alteration in the Cerrito de la Cruz deposits, Barker, Buenos Aires Province, Argentina. Göttinger Arbeiten zur Geologie und Paläontologie, 5: 1-6.

Dristas, J.A. and Martínez, J.C. 2007. Late Proterozoic unconformity-related hydrothermal iron deposits in the north Barker area (Tandilia ranges, Argentina). Neues Jahrbuch für Geologie und Paläontologie Abhandlungen, 246: 267-281.

Dristas, J.A., Martínez, J.C., Massonne, H.-J. and Pimentel, M.M. 2013. Mineralogical and geochemical characterization of a rare ultramafic lamprophyre in the Tandilia belt basement, Río de la Plata Craton, Argentina. Journal of South American Earth Sciences, 43: 46-61.

Fernández, R. R., Tessone, M., Etcheverry, R., Echeveste, H., Coriale, N. and Caballé, M. 2010. Interpretación de la distribución de elementos de las tierras raras en el basamento alterado de la zona de San Manuel, provincia de Buenos Aires. Revista de la Asociación Geológica Argentina, 67 (2): 216-230.

Frey, M. 1969. A mixed-layer paragonite/phengite of low-grade metamorphic origin. Contributions to Mineralogy and Petrology, 14: 63-65.

Frey, M. 1978. Progressive low-grade metamorphism of a black shale formation, Central Swiss Alps, with special reference to pyrophyllite and margarite bearing assemblages. Journal of Petrology, 19: 95-135.

Frey, M. 1987. Very low-grade metamorphism of clastic sedimentary rocks. In Frey, M. (ed.) Low temperature metamorphism, 8-58, Chapman and Hall, New York.

Frisicale, M.C. and Dristas, J.A. 1993. Alteración hidrotermal en el contacto entre el basamento y la secuencia sedimentaria, en el Cerrito de la Cruz, Tandilia. 12° Congreso Geológico Argentino and 2° Congreso de Exploración de Hidrocarburos, Actas 10: 222-228, Mendoza.

Fuhrman, M.L. and Lindsley, D.H. 1988. Ternary-feldspar modeling and thermometry. America Mineralogist, 73: 201-215.

Giorgetti, G., Monecke, T., Kleeberg, R. and Herzig, P.M. 2003. Intermediate sodium-potassium mica in hydrothermally altered rocks of the Waterloo deposits, Australia: a combined SEM-EMP-WRD-TEM study. Contributions to Mineralogy and Petrology, 146: 159-173.

Gómez Peral, L.E., Raigemborn, M.S. and Poiré, D. 2011. Petrología y evolución diagenética del Grupo Sierras Bayas, Sistema de Tandilia,

Argentina. Latin American Journal of Sedimentology and Basin Analysis, 18 (1): 3-41.

Guidotti, C.V., Sassi, F.P., Blenkoe, J.G. and Selverstone, J. 1994. The paragonite-muscovite solvus. I. P-T-X limits derived from the Na-K compositions of natural, quasibinary paragonite-muscovite pairs. Geochimica et Cosmochimica Acta, 58, 2269-2275.

Hartmann, L.A., Santos, J.O.S., Cingolani, C.A. and McNaughton, N.J. 2002. Two Paleoproterozoic orogenies in the evolution of the Tandilia belt, Buenos Aires, as evidenced by zircon U-Pb SHRIMP geochronology. International Geology Review, 44: 528-543.

Holland, T.J.B. and Powell, R. 1998. An internally consistent thermodynamic data set for phases of petrological interest. Journal of Metamorphic Geology, 16: 309-343.

Holland, T.J.B., Baker, J.M. and Powell, R. 1998. Mixing properties and activity-composition relationships of chlorites in the system MgO-FeO-Al_2O_3-SiO_2-H_2O. European Journal of Mineralogy, 10: 395-406.

Holland, T.J.B. and Powell, R. 2002. Activity-composition relations for phases in petrological calculations: an asymmetric multicomponent formation. Contributions to Mineralogy and Petrology, 145: 492-501.

Iacumin, M., Piccirillo, E.M., Girardi, V.A.V., Teixeira, W., Bellieni, G., Echeveste, H., Fernández, R., Pinese, J.P.P. and Ribot, A. 2001. Early Proterozoic calc-alkaline and Middle Proterozoic tholeiitic dyke swarms from central-eastern Argentina: petrology, geochemistry, Sr-Nd isotopes and tectonic implications. Journal of Petrology, 42: 2109-2143.

Iñíguez-Rodríguez, A.M., Del Valle, A., Poiré, D., Spalletti, L. and Zalba, P. 1989. Cuenca Precámbrica-Paleozoico inferior de Tandilia, Provincia de Buenos Aires. In Chebli, G. and Spalletti, L.A. (eds.) Cuencas sedimentarias argentinas, Serie Correlación Geológica 6, Instituto Superior de Correlación Geológica, Universidad Nacional de Tucumán, 245-263, Tucumán.

Jiang W.-T., Essene, E.J. and Peacor, D.R. 1990. Transmission electron microscopic study of coexisting pyrophyllite and muscovite: Direct evidence for the metastability of illite. Clays and Clay Minerals, 38: 225-240.

Jiang, W-T. and Peacor, D.R. 1993. Formation and modification of metastable sodium potassium mica, paragonite, and muscovite in the hydrothermally altered metabasites from the northern Wales. American Mineralogist, 78: 782-793.

Kisch, H.J. 1983. Mineralogy and petrology of burial diagenesis (burial metamorphism) and incipient metamorphism in clastic rocks. In Larsen, G. and Chilingar, G.V. (eds.) Diagenesis in sediments and sedimentary rocks 2, 289-493, Elsevier, New York, U.S.A.

Lackschewitz, K.S., Devy, C.W., Stoffers, P., Botz, R., Eisenhauer, A., Kummetz, M., Schmidt, and Singer, A. 2004. Mineralogical, geochemical and isotopic characteristic of hydrothermal alteration processes in active, submarine, felsic-hosted PACMANUS field, Manus Basin, Papua New Guinea. Geochimica et Cosmochimica Acta, 68: 4405-4427.

Li, G., Peacor, D.R., Merriman, R.J. and Roberts, B. 1994. The diagenetic to low-grade metamorphic evolution of matrix white micas in the system muscovite-paragonite in a mudrock from Central Wales, United Kingdom. Clay and Clay Minerals, 42 (4): 369-381.

Livi, K.J.T., Veblen, D.R., Ferry, J.M. and Frey, M. 1997. Evolution of 2:1 layered silicates in low-grade metamorphosed Liassic shale of Central Switzerland. Journal of Metamorphic Geology, 15 (3): 323-344.

Lo Pó, D. and Braga, R. 2014. Influence of ferric iron on phase equilibria in greenschist fácies assemblages: the hematite-rich metasedimentary rocks from the Monti Pisani (Northern Apennines). Journal of Metamorphic Geology, 32: 371-387.

Marchese, H. and Di Paola, E. 1975. Reinterpretación estratigráfica de la perforación de Punta Mogotes I, Provincia de Buenos Aires. Revista de la Asociación Geológica Argentina, 30: 44-52.

Martínez, J.C. and Dristas, J.A. 2007. Paleoactividad hidrotermal en la discordancia entre el Complejo Buenos Aires y la Formación La Tinta en el área de Barker, Tandilia. Revista de la Asociación Geológica Argentina, 62: 375-386.

Martínez, J.C., Dristas, J.A., Massonne, H.-J. and Theye, T. 2010. A hydrothermal clay mineral assemblage at the Late Proterozoic unconformity in the Buenos Aires Complex - La Tinta Formation, Barker area, Tandilia Ranges (Argentina). Clay Minerals, 45: 209-224.

Martínez, J.C., Dristas, J.A., van der Kerkhof, A.M., Wemmer, K., Massonne, H.-J., Theye, T. and Frisicale, M.C. 2013. Late-Neoproterozoic hydrothermal fluid activity in the Tandilia belt, Argentina. Revista de la Asociación Geológica Argentina, 70 (3): 410-426.

Massonne, H.-J. 2010. Phase relations and dehydration behaviour of calcareous sediments at very-low to low grade metamorphic conditions. Periodico di Mineralogia, 79: 21-43.

Massonne, H.-J., Dristas, J.A. and Martínez, J.C. 2012. Metamorphic evolution of the Río de la Plata Craton in the Cinco Cerros area, Buenos Aires Province, Argentina. Journal of South American Earth Science, 38: 57-70.

Merriman, R.J. 2002. Contrasting clay mineral assemblages in British Lower Palaeozoic slate belts: the influence of geotectonic setting. Clay Minerals, 37: 207-219.

Merriman, R.J. 2006. Clay mineral assemblages in British Lower Paleozoic mudrocks. Clay Minerals, 41: 473-512.

Merriman, R.J. and Frey, M. 1999. Patterns of very low-grade metamorphism in metapelitic rocks. In Frey, M. and Robinson, D. (eds.) Low-Grade Metamorphism, 61-107, Blackwell Science, Oxford, U.K.

Merriman, R.J. and Peacor, D.R. 1999. Very low-grade metapelites: mineralogy, microfabrics and measuring reaction progress. In Frey, M. and Robinson, D. (eds.) Low-Grade Metamorphism, 10-60, Blackwell Science, Oxford, U.K.

Monecke, T. Köhler, S. Kleeberg, R. Herzig, P.M. and Gemmell, J.B. 2001. Quantitative phase-analysis by Rietveld method using X-ray powder-diffraction data: application to the study of alteration halos associated with volcanic-rock-hosted massive sulphide deposits. Canadian Mineralogist, 39: 1617-1633.

Newman, A.C.D. and Brown, G. 1987. The chemical constitution of clays. In Newman, A.C.D. (eds.) Chemistry of Clay and Clay Minerals, Monograph 6, Mineralogical Society, 1-48, London, U.K.

Pankhurst, R.J., Ramos, A. and Linares, E. 2003. Antiquity of the Río de la Plata Craton in Tandilia, southern Buenos Aires province, Argentina. Journal of South American Earth Sciences, 16: 5-13.

Parra, T., Vidal, O. and Agard, P. 2002. A thermodynamic model for Fe-Mg dioctahedral K white micas using data from phase-equilibrium experiments and natural pelitic assemblages. Contributions to Mineralogy and Pe-

trology, 143: 706-732.

Poiré, D.G. 1987. Mineralogía y sedimentología de la Formación Sierras Bayas en el núcleo septentrional de las sierras homónimas, Partido de Olavarría, Provincia de Buenos Aires. Tesis doctoral, Facultad de Ciencias Naturales y Museo, Universidad Nacional de La Plata (inédita), 271 p., La Plata.

Poiré, D. G. and Spalletti, L. A. 2005. La cubierta sedimentaria Precámbrica-Paleozoica inferior del Sistema de Tandilla. In Barrio, R.E., Etcheverry, R.O. Caballé, M.F. and Llambías, E. (eds.), Relatorio 4, Geología y recursos minerales de la provincia de Buenos Aires, 15° Congreso Geológico Argentino, 51-68, La Plata.

Regalia, G.M. 1987. Carácteres geológicos del área de San Manuel, Sierras Septentrionales de la provincia de Buenos Aires. Revista de la Asociación Geológica Argentina, 42 (1-2): 143-152.

Renne, P.R., Mundil, R., Balco, G., Min, K. and Ludwig, K.R. 2010. Joint determination of 40K decay constants and 40Ar*/40K for the Fish Canyon sanidine standard, and improved accuracy for $^{40}Ar/^{39}Ar$ geochronology. Geochimica et Cosmochimica Acta, 74: 5349-5367.

Rieder, M., Cavazzini, G., D'Yakonov, Y.S., Frank- Kamenetskii, V.A., Gottardi, G., Guggenheim, S., Koval, P.V., Müller, G., Neiva, A.M.R., Radoslovich, E.W., Robert, J-L., Sassi, F.P., Takeda, H., Weiss, Z. and Wones, D.R. 1998. Nomenclature of the micas. Clays and Clay Minerals, 46: 586-595.

Ruiz Cruz, M.D., Morata, D., Puga, E., Aguirre, L. and Vergara, M. 2004. Microstructures and interlayering in pyrophyllite from the Coastal Range of central Chile: evidence of a disequilibrium assemblage. Clay Minerals, 39: 439-452.

Sellés-Martínez, J. 1993. Lineamientos estructurales y evolución extensional de la plataforma Neoproterozoica-Eopaleozoica de las Sierras Septentrionales de la provincia de Buenos Aires, Argentina. Revista Brasileira de Geociências, 23 (3): 289-295.

Shau, Y.-H., Feather, M.E., Essene, E.J. and Peacor, D.R. 1991. Genesis and solvus relations of submicroscopically intergrown paragonite and phengite in a blueschist from northern California. Contributions to Mineralogy and Petrology, 106: 367-378.

Tajcmanová, L., Connolly, J.A.D. and Cesare, B. 2009. A thermodynamic model for titanium and ferric iron solution in biotite. Journal of Metamorphic Geology, 27: 153-164.

Teixeira, W., Pinese, J.P.P., Iacumin, M., Girardi, V.A.V., Piccirillo, E.M., Echeveste, H., Ribot, A., Fernandez, R., Renne, P.R. and Heaman, L.M. 2002. Calc-alkaline and tholeiitic dyke swarms of Tandilia, Rio de la Plata craton, Argentina: U-Pb, Sm-Nd, and Rb-Sr, $^{40}Ar/^{39}Ar$ data provide new clues for intraplate rifting shortly after the Trans-Amazonian Orogeny. Precambrian Research, 119: 329-353.

Velde, B. 1985. Clay minerals: a physico-chemical explanation of their occurrence: Developments in Sedimentology, 40, Elsevier, 427 p., Amsterdam.

Zalba, P.E., Poiré, D.G., Andreis, R.R. and Iñiguez-Rodriguez, A.M. 1992. Precambrian and lower Paleozoic paleoweathering records and paleosurfaces of the Tandilia system, Buenos Aires province, Argentina. Mineralogical and geochemical records of paleoweathering. Mémoire des Sciences de la Terre, 18: 153-161.

Zalba, P.E. and Andreis, R.R. 1998. Basamento saprolitizado y secuencia sedimentaria suprayacente en San Manuel, Sierras Septentrionales de Buenos Aires, Argentina. 7° Reunión Argentina de Sedimentología, Actas: 143-155, Salta.

Zalba, P.E., Manassero, M., Laverret, E., Beaufort, D., Meunier, A. and Segovia, L. 2007. Middle Permian telodiagenetic processes in Neoproterozoic sequences, Tandilia System, Argentina. Journal of Sedimentary Research, 77: 525-538.

Zen, E-An. 1960. Metamorphism of lower Paleozoic rocks in the vicinity of the Taconic range in West-central Vermont. American Mineralogist, 45: 129-175.

Received: 27 de agosto, 2014
Accepted: 5 de abril, 2015